Complementary Shapes in Columnar Liquid Crystals: Structural Control in Homo- and Heteronuclear Bimetallic Assemblies

André G. Serrette, Chung K. Lai, and Timothy M. Swager*,†

Department of Chemistry, University of Pennsylvania, Philadelphia, Pennsylvania 19104-6323

Received July 29, 1994. Revised Manuscript Received October 4, 1994®

A comprehensive study of the liquid-crystalline properties of 51 bimetallic compounds based upon 1,3,5-triketonate and 1,3,5,7-tetraketonate ligands is reported. These materials are liquid crystalline when six or more side chains are appended to the mesogenic core, and only columnar phases were observed. Most of the liquid crystals were homonuclear dicopper complexes. Schiff-base derivatives of some of the triketones allowed for the synthesis of heteronuclear bimetallic liquid crystals. The NiCu and NiPd Schiff-base complexes are the first heteronuclear liquid crystals with proximate (strongly interacting) metal centers. Other heteronuclear complexes investigated were not liquid crystalline due to the tendency to retain coordinated solvent or to form strongly associated structures in the absence of axial ligands. The use of complementary shapes was demonstrated as a means to generate average relative organizations (correlations) between the complexes. The presence of these correlated structures was shown through comparisons of the structures, phase behavior, and the immiscibility between materials having the same phase but different shapes. Correlated structures were shown which produce average rotations of 90° and 180° between nearest-neighbor molecules. A crystal structure of one compound confirmed that a similar superstructure was exhibited in the solid state. In addition, it was found that the correlated structures exhibit relatively short (3.29 Å) correlations between the mesogens, thereby allowing for strong intermolecular interactions. The ability to control the orientation and relative position of transition metal centers in liquid crystals has applications in the design of new liquid-crystalline materials with useful magnetic and electronic properties.

Introduction

Modern synthetic chemistry has mainly concentrated on the systematic design of structures that tune various molecular properties. The exploitation of this knowledge to produce important molecular materials requires new rational design methodologies which produce assemblies with selected local and extended interactions. A popular route to these advanced materials is to design supermolecular assemblies, an approach which has many analogies to the finely tuned functions of highly organized biological systems.[1-3] In these systems, weak chemical bonding, such as hydrogen bonding[1,4] or dative coordinative interactions between transition metals,[5] can be used to effect structural control. This report describes a different approach in which liquid crystalline bimetallic complexes with complementary molecular shapes are used to produce materials with specific intermolecular associations and superstructures.[6]

We have been interested in mesomorphic materials containing transition metals (metallomesogens)[7,8] because these materials promise to expand the range of technological applications and properties exhibited by liquid crystals. Efforts in this area have resulted in mononuclear complexes which display most of the known liquid crystalline phase types.[8] However, it is well-known that multinuclear metal complexes often give rise to important physical properties such as ferromagnetic coupling[9] and mixed oxidation states,[10] which are not possible in simple mononuclear complexes. The incorporation of such properties is a

† Office of Naval Research Young Investigator 1992-1995, NSF Young Investigator 1992-1997, DuPont Young Professor Grantee 1993-1996, Alfred P. Sloan Research Fellow 1994-1996.

® Abstract published in *Advance ACS Abstracts*, November 1, 1994.

(1) (a) Lehn, J.-M. *Angew. Chem., Int. Ed. Engl.* **1990**, *29*, 1304. (b) Lehn, J.-M. *Science* **1993**, *260*, 1762.

(2) Vögtle, F. *Supramolecular Chemistry: An Introduction*; John Wiley and Sons: Chichester, 1993.

(3) For reviews on self-assembly see: (a) Whitesides, G. M.; Mathias, J. P.; Seto, C. T. *Science* **1992**, *254*, 1312. (b) Lindsey, J. S. *New J. Chem.* **1991**, *15*, 153.

(4) For recent work see: (a) Zerkawski, J. A.; Whitesides, G. M. *J. Am. Chem. Soc.* **1994**, *116*, 4298. (b) Mathias, J. P.; Simanek, E. E.; Zerkawski, J. A.; Seto, C. T.; Whitesides, G. M. *J. Am. Chem. Soc.* **1994**, *116*, 4316. (c) Geib, S. J.; Vicent, C.; Fan, E.; Hamilton, A. D. *Angew. Chem., Int. Ed. Engl.* **1993**, *32*, 119.

(5) (a) Constable, E. *Angew. Chem., Int. Ed. Engl.* **1991**, *30*, 1450 and references therein. (b) Constable, E.; Hannon, M. J.; Tocher, D. A. *Angew. Chem., Int. Ed. Engl.* **1992**, *31*, 230. (c) Abrahams, B. F.; Hoskins, B. F.; Robson, R. *J. Am. Chem. Soc.* **1991**, *113*, 3606. (d) Chambron, J-C.; Dietrich-Buchecker, C. O.; Nierengarten, J.-F.; Sauvage, J.-P. *J. Chem. Soc., Chem. Commun.* **1993**, 801. (e) Leize, E.; Dorsselaer, A. V.; Krämer, R.; Lehn, J.-M. *J. Chem. Soc., Chem. Commun.* **1993**, 990. (f) Serrette, A. G.; Swager, T. M. *J. Am. Chem. Soc.* **1993**, *115*, 8879.

(6) We have communicated part of this work previously. Lai, C. K.; Serrette, A. G.; Swager, T. M. *J. Am. Chem. Soc.* **1992**, *114*, 7949.

(7) (a) *Thermotropic Liquid Crystals: Critical Reports on Applied Chemistry*; Gray, G. W., Ed., Society of Chemical Industry: London, 1987; Vol. 22. (b) Chandrasekhar, S. *Liquid Crystals*, 2nd ed., Cambridge University Press: Cambridge, 1992.

(8) For reviews see: (a) Giroud-Godquin, A. M.; Maitlis, P. M. *Angew. Chem., Int. Ed. Engl.* **1991**, *30*, 375. (b) Hudson, S. A.; Maitlis, P. M. *Chem. Rev.* **1993**, *93*, 861. (c) Espinet, P.; Esteruelas, M. A.; Oro, L. A.; Serrano, J. L.; Sola, E. *Coord. Chem. Rev.* **1992**, *117*, 215.

(9) (a) Kahn O. *Comments on Inorg. Chem.* **1984**, *3*, 105-132. (b) Kahn O. *Angew Chem., Int. Ed. Engl.* **1985**, *24*, 834-850. (c) Kahn O. *Molecular Magnetism*; VCH Publishers: New York, 1993.

(10) (a) Creutz C. In *Prog. Inorg. Chem.* **1983**, *30*, 1. (b) Richardson, D. E.; Taube, H. *Coord. Chem. Rev.* **1984**, *60*, 107.

0897-4756/94/2806-2252$04.50/0

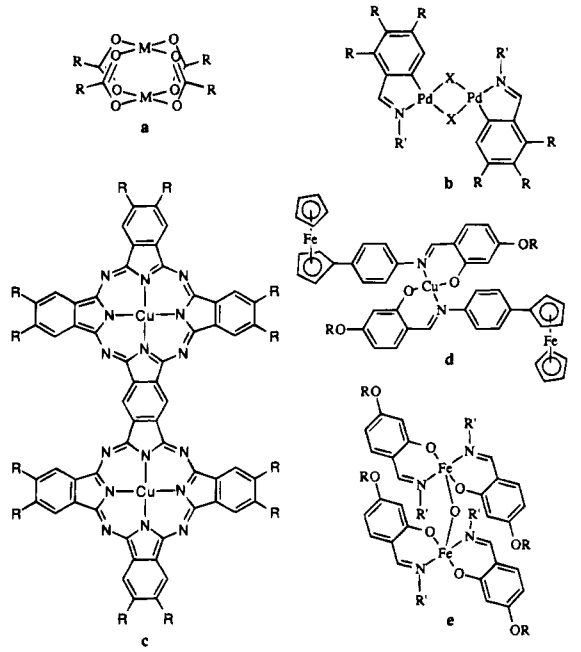

Figure 1. Structural representations of previously investigated polymetallic liquid crystals. Homonuclear bimetallic complexes which bridging carboxylates (a), cyclometalated palladium complexes (b), a fused copper phthalocyanine (c), a mixed metal ferrocene/copper salicylaldimine complex (d), and a μ-oxoiron complex (e). R and R' represent groups containing long alkane chains.

significant step toward producing liquid crystals with extended magnetic interactions and high electrical conductivity. Despite this potential, few structural types of liquid crystals containing multiple metal centers have been investigated. Representative structures, shown in Figure 1, are homobimetallic complexes with bridging carboxylates,[11] cyclometalated palladium complexes,[12] a fused copper phthalocyanine,[13] a mixed metal ferrocene/copper salicylaldimine complex,[14] and a μ-oxoiron complex.[15] The ferrocene/copper salicylaldimine complex is the only example of a heteronuclear metallomesogen prior to the work discussed herein.

We describe herein our investigations of the supermolecular structures and liquid crystalline properties of 51 new bimetallic complexes with seven different structural types shown in Figure 2. Our results illustrate a general approach in which complementary shapes can be used to design liquid crystals with specific organizations between the constituent molecules. All of the reported compounds have a polyketonate structure, and the coordination chemistry of nonmesogenic analogues of these structures have been previously investigated, most notably by the groups of Lintvedt[16] and Fenton.[17] These prior investigations have shown that polyketonate complexes display diverse coordination chemistries and physical properties. It has also been shown that close proximity of the metal centers in the triketonates can lead to strong magnetic coupling[16,18] and electrochemical redox manifolds.[19] In addition, the compartmental nature of the Schiff-base ligands provides a useful approach to the formation of heteronuclear bimetallic complexes with strong magnetic coupling.[9,17,20] Heteronuclear bimetallic complexes are of particular interest since they have been shown by Kahn[9] to be versatile building blocks for the formation of molecular ferrimagnetic materials.

Results and Discussion

Synthesis. All the triketonate and tetraketonate ligands **8**–**13** were prepared (Schemes 1 and 2) using cross-Claisen condensation reactions.[21] Triketonate, **10**, which bears five side chains, required the preparation of an intermediate 1-(3′,4′,5′-trialkyloxyphenyl)-1,3-butanedione which is then condensed further with a 3,4-dialkyloxyphenyl methyl ester fragment. Condensation of the triketones **11** and the tetraketones **13** with diamines in chloroform produced the Schiff-base ligands **14** and **15** (Scheme 3). Spectroscopic characterization (NMR and IR) of all of the ligands is complicated by the fact that the molecules exist in different keto–enol tautomeric forms. Additionally, it is possible that other conformational effects may lead to the observed spectra; however, this seems unlikely considering the steric requirements of the pendant phenyl rings. ^{1}H NMR of the triketones in chloroform showed enol forms, **A** and **B**,

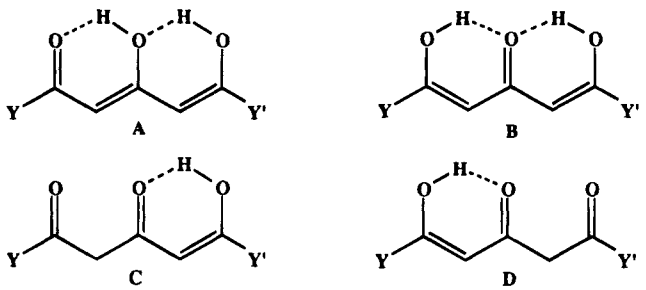

to be dominant. Diagnostic resonances are the hydroxyl hydrogens of **A** and **B** which are observed between 10 and 17 ppm and the olefinic methine hydrogens connected to the central carbons of the diketone moieties which occur between 4.5 and 6.5 ppm. For the sym-

(11) (a) Giroud-Godqin A. M.; Marchon, J. C.; Guillon, D.; Skoulios, A. *J. Phys. Chem.* **1986**, *90*, 5502. (b) Maldivii, P.; Giroud-Godquin, A.-M.; Marchon, J.-C.; Guillon, D.; Skoulios, A. *Chem. Phys. Lett.* **1989**, *157*, 552. (c) Cayton, R. H.; Chisholm, M. H.; Darrington, F. D. *Angew. Chem., Int. Ed. Engl.* **1990**, *29*, 1481. (d) Barberá, J.; Esteruelas, M. A.; Levelut, A. M.; Oro, L. A.; Serrano, J. L.; Sola, E. *Inorg. Chem* **1992**, *31*, 732. (e) Ohta, K.; Ema, H.; Yamamoto, I.; Matsuzaki, K. *Liq. Cryst.* **1988**, *3*, 1671. (f) Bonnet, L.; Cukiernik, F. D.; Maldivi, P.; Giroud-Godquin, A.-M.; Marchon, J.-C.; Ibn-Elhaj, M.; Guillon, D.; Skoulios, A. *Chem. Mater.* **1994**, *6*, 31.

(12) (a) Ghedini M.; Longeri, M.; Bartolino, R. *Mol. Cryst. Liq. Cryst.* **1982**, *84*, 207. (b) Rox, M. B.; Ruiz, N.; Serrano, J. L.; Espinet, P. *Liq. Cryst.* **1991**, *9*, 77. (c) Praefcke, K.; Singer, D.; Gündogan, B. *Mol. Cryst. Liq. Cryst.* **1992**, *223*, 181. (d) Praefcke, K.; Gündogan, B. *Chem. Ber.* **1993**, *126*, 1253. (e) Usol'tseva, N.; Praefcke, K.; Singer, D.; Gündogan, B. *Liq. Cryst.* **1994**, *16*, 601.

(13) Lelievre, D.; Bosio, L.; Simon, J.; Andre', J. J.; Bensebaa, F. *J. Am. Chem. Soc.* **1992**, *114*, 4475.

(14) Galyametdinov, Y.; Kadkin, O. N. .; Ovchinnikov, I. V. *Izu. Akad. Nauk. SSSR, Ser. Khim.* **1990**, *N12*, 2462.

(15) Galyametdinov, Y.; Ivanova, G.; Griesar, K.; Prosvirin, A.; Ovchinnikov, I.; Haase, W. *Adv. Mater.* **1992**, *4*, 739.

(16) (a) Glick, M. D.; Lintvedt, R. L. *Prog. Inorg. Chem.* **1976**, *21*, 233 and references therein. (b) Lintvedt, R. L.; Tomlonovic, B.; Fenton, D. E.; Glick, M. D. In *Adv. Chem.* **1976**, *No. 150*, p 407, American Chemical Society.

(17) Casellato, U.; Vigato, P. A.; Fenton, D. E.; Vidali, M. *Chem. Soc. Rev.* **1979**, *8*, 199 and references therein.

(18) (a) Baker, D.; Dudley, C. W.; Oldham, C. *J. Chem. Soc. A* **1970**, 2608. (b) Kuszaj, J. M.; Tomlonovic, B.; Murtha, D. P.; Lintvedt, R. L.; Glick, M. D. *Inorg. Chem.* **1973**, *12*, 1297. (c) Lintvedt, R. L.; Borer, L. L.; Murtha, D. P.; Kuszaj, J. M.; Glick, M. D. *Inorg. Chem.* **1974**, *13*, 18. (d) Lintvedt, R. L.; Glick, M. D.; Tomlonovic, B. K.; Gavel, D. P.; Kuszaj, J. M. *Inorg. Chem.* **1976**, *15*, 1633. (e) Guthrie, J. W.; Lintvedt, R. L.; Glick, M. D. *Inorg. Chem.* **1980**, *19*, 2949. (f) Heeg, M. J.; Mack, J. L.; Glick, M. D.; Lintvedt, R. L. *Inorg. Chem.* **1981**, *20*, 833. (g) Wishart, J. F.; Ceccarelli, C.; Lintvedt, R. L.; Berg, J. M.; Foley, D. P.; Frey, T.; Hahn, J. E.; Hodgson, K. O.; Weis, R. *Inorg. Chem.* **1983**, *22*, 1667.

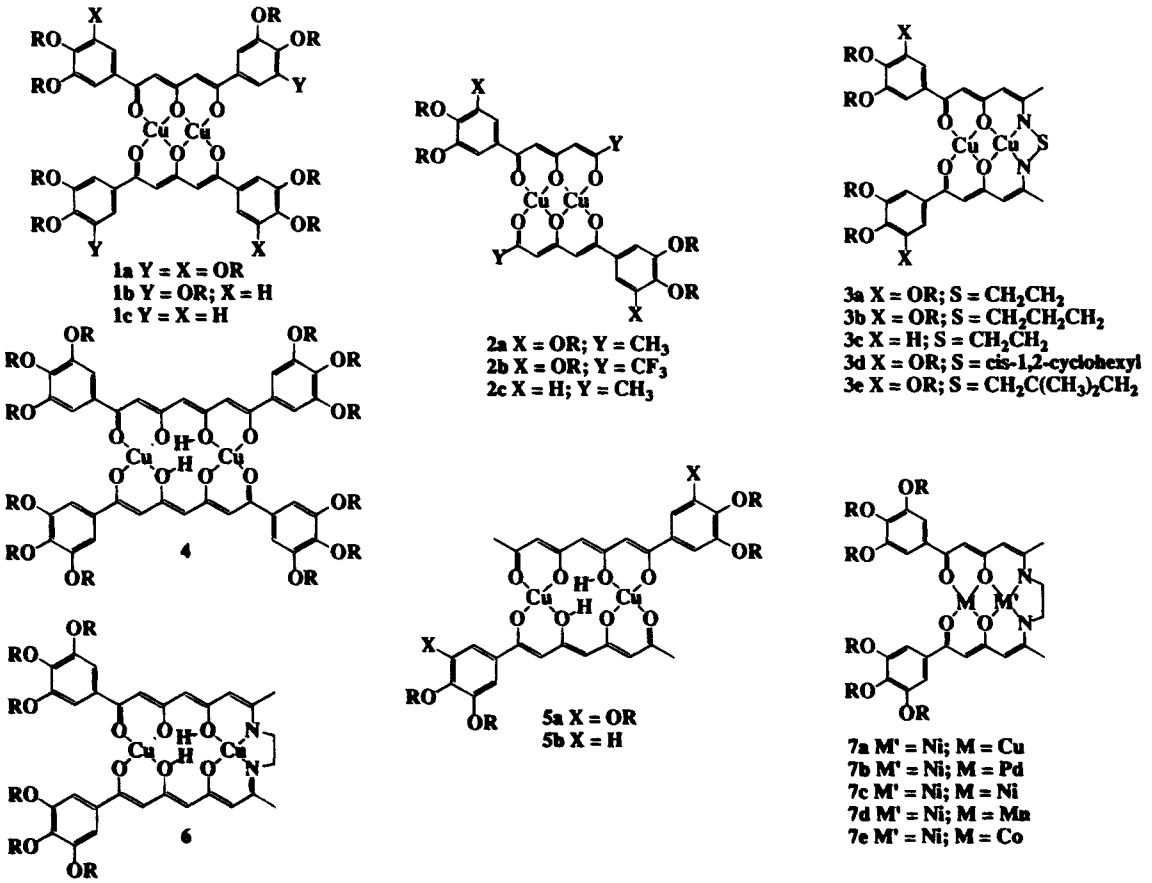

Figure 2. Structures of the seven series of compounds studied. R = $(CH2)_nH$.

Scheme 1[a]

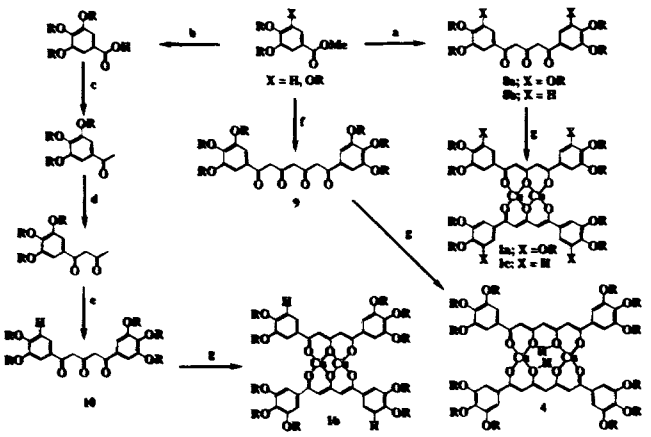

[a] 0.5 equiv of acetone, 6.0 equiv of NaH, DME, reflux 24 h, 85–90%. [b] 1.1 equiv of NaOH, THF/H_2O (8/1), reflux 3 h, 98%. [c] 3.0 equiv of MeLi, THF, room temperature 4 h, 94%. [d] 3.0 equiv of NaH, ethylacetate, reflux 24 h, 89%. [e] 1.0 equiv of 3,4-tridecyloxybenzoic acid ethyl ester, 3.0 equiv of NaH, DME, reflux 24 h, 93%. [f] 0.5 equiv of 2,4-pentadione, 6.0 equiv of NaH, DME, reflux 24 h, 83%. [g] 1.1 equiv of $Cu(OAc)_2(H_2O)$, $CHCl_3$/EtOH (1/4), 70 °C, 3 h, 73–93%.

metrically substituted triketone (Y = Y' = Ar) such as **8**, two olefinic hydrogen resonances were observed indicating that only tautomeric structures **A** and **B** are present. In the case of **11** (Y ≠ Y') four olefinic hydrogen resonances are observed, and the presence of keto structures **C** and/or **D** yields two additional resonances between 3 and 4 ppm. Compound **14**, comprising two fragments of **11** joined by a diamine bridge, displays more complicated spectra with six olefinic resonances. Both keto and enol forms were observed in the tetraketones in approximately equal amounts.

The dicopper complexes were prepared in a straightforward procedure by treatment of the ligands with excess cupric acetate in chloroform/methanol solutions. All of these compounds are paramagnetic, and the ^1H NMR spectra display only alkyloxy signals. Apparently, the close proximity of the other protons to the copper centers renders them NMR invisible. Compounds **1a–c** were obtained as green crystalline materials which showed strong infrared absorptions at 1588–94 cm^{-1}, characteristic of coordinated carbonyls in triketonate moieties. Carbonyl bands at 1677–1686 cm^{-1} which are indicative of the free ligand and monometalated ligands were not observed. Elemental analysis and mass spectrometry also confirmed the bimetallic identity of the complexes. Complexes **2a–c** are also green, and similar infrared, elemental, and mass spectrometric analysis all support the assigned structures. Nonmesogenic triketonates related to **2** have been previously shown to assemble as pseudo-trans regioisomers,[16b] and we as-

(19) (a) Fenton, D. E.; Schroeder, R. R.; Lintvedt, R. L. *J. Am. Chem. Soc.* **1978**, *100*, 6367. (b) Lintvedt, R. L.; Kramer, L. S. *Inorg. Chem.* **1983**, *22*, 796. (c) Lintvedt, R. L.; Ranger, G.; Schoenfelner, B. A. *Inorg. Chem.* **1984**, *23*, 688. (d) Lintvedt, R. L.; Schoenfelner, B. A.; Ceccarelli, C.; Glick, M. D. *Inorg. Chem.* **1984**, *23*, 2867. (e) Lintvedt, R. L.; Rupp, K. A.; Heeg, M. J. *Inorg. Chem.* **1988**, *27*, 331. (f) Lintvedt, R. L.; Zehetmair, J. K. *Inorg. Chem.* **1990**, *29*, 2204. (g) Lintvedt, R. L.; Lynch, W. E.; Zehetmair, J. K. *Inorg. Chem.* **1990**, *29*, 3009.

(20) (a) Fenton, D. E.; Gayda, S. E. *Inorg. Chim. Acta.* **1975**, *14*, L11. (b) Lintvedt, R. L.; Glick, M. D.; Tomlonovic, B. K.; Gavel, D. P. *Inorg. Chem.* **1976**, *15*, 1646. (c) Glick, M. D.; Lintvedt, R. L.; Gavel, D. P.; Tomlonovic, B. K. *Inorg. Chem.* **1976**, *15*, 1654. (d) Fenton, D. E.; Gayda, S. E. *J. Chem. Soc., Dalton* **1977**, 2109. (e) Adams, H.; Bailey, N. A.; Fenton, D. E.; Gonzalez, M. S. L.; Phillips, C. A. *J. Chem. Soc., Dalton* **1983**, 371. (f) Lintvedt, R. L.; Kramer, L. S.; Ranger, G.; Corfield, P. W.; Glick, M. D. *Inorg. Chem.* **1983**, *22*, 3580.

(21) Miles, M. L.; Harris, T. M.; Hauser, C. R. *J. Org. Chem.* **1965**, *30*, 1007.

Scheme 2[a]

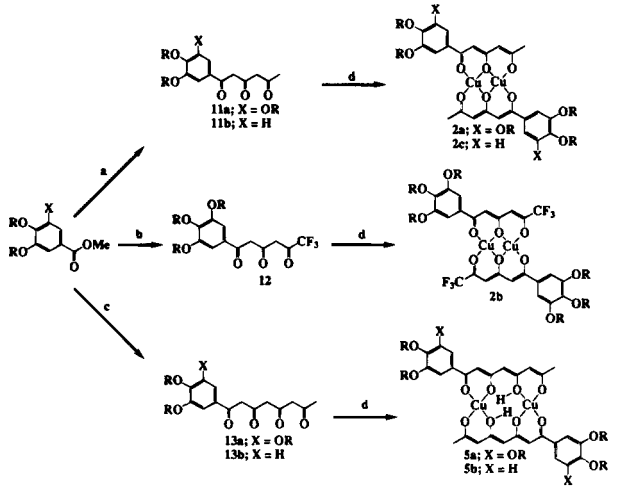

[a] 1.0 equiv of 2,4-pentadione, 3.0 equiv of NaH, DME, reflux 24 h, 89–90%. [b] 1.0 equiv of 1,1,1-trifluoro-2,4-pentanedione, 3.0 equiv of NaH, DME, reflux 24 h, 82%. [c] 1.0 equiv of 1,3,5-heptatrione, 3.0 equiv of NaH, DME, reflux 24 h, 62–73%. [d] 1.1 equiv of $Cu(OAc)_2(H_2O)$, $CHCl_3$/MeOH (1/4), 70 °C, 3 h, 67–95%.

Scheme 3[a]

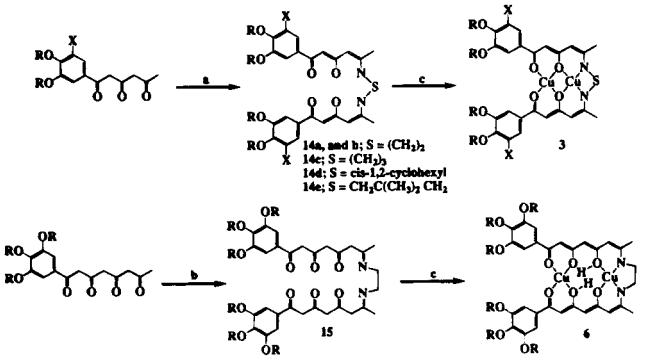

[a] 0.5 equiv of NH_2SNH_2, $CHCl_3$, room temperature, 12 h, 81–91%. [b] 0.5 equiv of $H_2NC_2H_4NH_2$, $CHCl_3$, room temperature, 12 h, 79%. [c] 2.0 equiv of $Cu(OAc)_2(H_2O)$, $CHCl_3$/MeOH (1/4), 70 °C, 3 h, 83–95%.

sume a similar structure here since this arrangement should be further enhanced by the greater steric requirements of the alkyloxy side chains.

The tetraketone-based ligands have the potential to complex three transition-metal ions. However, mass spectrometry indicates that only dicopper complexes **4** and **5** are produced even when reacted with excess $Cu(OAc)_2$. The assigned structure is supported by infrared spectroscopy which shows carbonyls only to be present in coordinated form with bands at 1580–88 cm^{-1}. Additionally, a broad OH stretching band at 3468 cm^{-1} is assigned to the central diketone moiety which resides as an enol tautomer. The absence of IR bands characteristic of uncomplexed carbonyls indicates that other possible regioisomers of **4** and **5** are not formed, and these results are consistent with previous investigations on nonmesogenic systems.[22] The structure assigned to **6** is supported by similar data.

The Schiff-base ligands provide two different sites for metal complexation, and thus these so-called compartmental ligands are well suited for the preparation of heteronuclear bimetallic complexes.[20] These preparations are best accomplished in a stepwise fashion wherein the ligand is first reacted with a metal ion which selectively chelates in the all-oxygen-containing site (O_2O_2) or the site containing the Schiff base (N_2O_2). Nickel is particularly well-behaved in this regard, and reaction with $Ni(OAc)_2$ produces solely the N_2O_2 complex **16** (Scheme 4). The structure of this square-planar diamagnetic Ni^{2+} complex is confirmed by NMR spectroscopy which shows shifts in the ethylene bridge of the Schiff base and changes in the resonances of methyl β to the nitrogens, both of which are consistent with values reported for nonmesogenic analogs.[23] Again the ^1H NMR is complicated by multiple resonances originating from the presence of different tautomeric forms. The vacant O_2O_2 coordination site in **16** is confirmed by carbonyl bands in the infrared at 1671 cm^{-1}. Further treatment of **16** with a variety of other metal salts produces heteronuclear bimetallic complexes in which the O_2O_2 site is occupied by a Cu, Co, Ni, Pd, or Mn ion (Scheme 4). The occupation of both coordination sites is confirmed by IR and elemental analysis. Mass spectrometric analysis also confirms the heteronuclear bimetallic nature of all of the complexes of series **7**. In contrast to the dicopper complexes, some members of series **7** are isolated with methanol coordinated in their axial positions. Thermogravimetric analysis of the Ni/Ni, Ni/Mn, and Ni/Co complexes indicates that the methanol is liberated at temperatures above 75 °C.

Scheme 4[a]

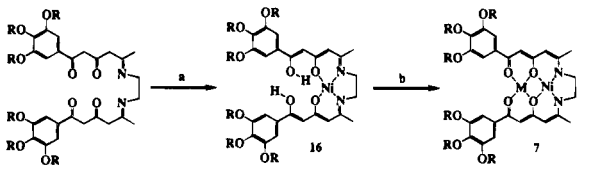

[a] 1.0 equiv of $Ni(OAc)_2(4H_2O)$, THF/MeOH (1/4), 70 °C, 0.5 h, 81%. [b] 1.0 equiv of $M(OAc)_2$ or $M(ClO4)_2$, THF/MeOH (1/4), 70 °C, 3 h, 44–67% (M = Ni, Cu, Pd, Co, and Mn).

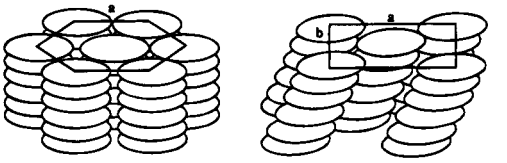

Figure 3. Schematic drawings of a hexagonal columnar phase (D_{hd}) left, and a rectangular columnar phase (D_{rd}) with $C_{2/m}$ symmetry right.

Liquid-Crystalline Behavior. The liquid-crystalline properties of all mesomorphic substances are determined by a balance between dispersive forces and attractive forces between the molecules.[7] For bimetallomesogens **1**–**7** the dispersive forces arise from highly dynamic motions of the alkyloxy side chains and oscillatory motions of the phenyl groups. The attractive forces are a combination of dipolar forces which is present in all thermotropic liquid crystals and weak intermolecular dative bonding which are often present in metallomesogens.[8] All of the liquid-crystalline complexes reported in this study display columnar phases.[24] In this type of mesophase the molecules assemble into columns which organize into a two-dimensional superlattice (Figure 3). While the correlation lengths of the superlattice can be large, the correlations between and

(22) Andrelczyk, B.; Lintvedt, R. L. *J. Am. Chem. Soc.* **1972**, *94*, 8633.

(23) Fenton, D. E.; Gayda, S. E. *J. Chem. Soc., Dalton* **1977**, 2101.

Table 1. Phase Behavior of 1a–c[a]

compound	n	phase behavior of complexes
1a	5	$K_1 \underset{85.8\ (0.3)}{\overset{94.7\ (0.3)}{\rightleftharpoons}} K_2 \underset{95.0\ (0.4)}{\overset{103.0\ (0.5)}{\rightleftharpoons}} K_3 \underset{119.2\ (0.7)}{\overset{138.3\ (1.0)}{\rightleftharpoons}} K_4 \underset{156.5\ (3.2)}{\overset{173.0\ (3.4)}{\rightleftharpoons}} D_{rd} \underset{208.6\ (0.9)}{\overset{210.9\ (1.0)}{\rightleftharpoons}} I$
	6	$K \underset{76.4\ (3.3)}{\overset{97.6\ (5.1)}{\rightleftharpoons}} D_{rd} \underset{214.3\ (1.2)}{\overset{217.6\ (1.3)}{\rightleftharpoons}} I$
	7	$K \underset{80.1\ (3.6)}{\overset{96.2\ (4.4)}{\rightleftharpoons}} D_{rd} \underset{189.4\ (1.1)}{\overset{192.6\ (1.2)}{\rightleftharpoons}} I$
	8	$K_1 \underset{42.7\ (5.6)}{\overset{56.8\ (6.1)}{\rightleftharpoons}} K_2 \underset{55.8\ (5.1)}{\overset{72.1\ (4.6)}{\rightleftharpoons}} D_{rd} \underset{187.5\ (1.4)}{\overset{190.3\ (1.7)}{\rightleftharpoons}} I$
	10	$K \underset{55.2\ (10.8)}{\overset{67.3\ (9.5)}{\rightleftharpoons}} D_{rd} \underset{177.9\ (1.4)}{\overset{181.2\ (1.4)}{\rightleftharpoons}} I$
	12	$K \underset{38.8\ (25.4)}{\overset{55.5\ (24.7)}{\rightleftharpoons}} D_{hd} \underset{162.1\ (1.7)}{\overset{164.1\ (1.8)}{\rightleftharpoons}} I$
	14	$K \underset{38.0\ (25.4)}{\overset{64.7\ (20.2)}{\rightleftharpoons}} D_{hd} \underset{145.7\ (1.4)}{\overset{148.2\ (1.5)}{\rightleftharpoons}} I$
	16	$K \underset{58.8\ (36.7)}{\overset{73.1\ (32.6)}{\rightleftharpoons}} D_{hd} \underset{137.8\ (1.1)}{\overset{140.5\ (1.0)}{\rightleftharpoons}} I$
1b	10	$K \underset{86.5\ (4.8)}{\overset{120.5\ (4.9)}{\rightleftharpoons}} D_{hd} \underset{189.9\ (1.4)}{\overset{192.3\ (1.4)}{\rightleftharpoons}} I$
1c	7	$K \underset{155.1\ (10.5)}{\overset{170.4\ (10.8)}{\rightleftharpoons}} D_{hd} \xrightarrow{255.0} I_d$
	10	$K \underset{129.1\ (17.8)}{\overset{151.5\ (17.5)}{\rightleftharpoons}} D_{hd} \xrightarrow{230.6} I_d$
	16	$K \underset{116.6\ (21.0)}{\overset{135.2\ (22.1)}{\rightleftharpoons}} D_{hd} \underset{186.7\ (0.3)}{\overset{187.3\ (0.3)}{\rightleftharpoons}} I$

[a] The transition temperatures (°C) and enthalpies, in parentheses (kcal/mol), were determined by DSC (scan rate 10 °C/min) and optical microscopy are given above and belowthe arrows. The number of carbon atoms in the alkyl chain is represented by n, and I, K, D_{rd}, and D_{hd} represent isotropic, crystal, discotic rectangular disordered, and discotic hexagonal disordered, phases, respectively. I_d indicates an isotropic phase with decomposition.

molecules within the columns are liquid-like. The superlattice types of interest for the work reported herein have hexagonal and rectangular symmetry and are generally labeled as D_{hd} and D_{rd}, respectively.[24] In a D_{hd} phase, the mesogenic plane is generally perpendicular to the columns axis, and a rotationally averaged shape of the molecules gives a circular projection along the column's axis. A distortion from a D_{hd} to a D_{rd} superstructure results when the molecules project a elliptical shape along the column's axis. As shown in Figure 3, the D_{rd} distortion is generally accomplished by a tilting of the molecules within the columns. A number of tilted symmetries are possible, and in Figure 3 we show a ($C_{2/m}$) structure which is the simplest organization. The thermochemical data and phase behavior of all of the complexes are given in Tables 1–4.

All of the compounds of series **1** exhibit liquid-crystalline phases with wide stability ranges (Table 1). The crystal-to-liquid crystal (melting) transition enthalpies are variable (3–37 kcal/mol) and occur at relatively mild temperatures (50–100 °C) with the **1a** $n = 12$ derivative melting at the lowest temperature. The

Table 2. Phase Behavior of Series 2[a]

compound	n	phase behavior
2a	5	$K \underset{86.2\ (8.4)}{\overset{141.1\ (9.7)}{\rightleftharpoons}} D_{hd} \xrightarrow{265.0} I_d$
	6	$K \underset{95.9\ (12.2)}{\overset{138.6\ (12.4)}{\rightleftharpoons}} D_{hd} \xrightarrow{247.2} I_d$
	7	$K_1 \underset{32.3\ (1.5)}{\overset{58.0\ (3.8)}{\rightleftharpoons}} K_2 \underset{96.2\ (11.5)}{\overset{128.4\ (11.9)}{\rightleftharpoons}} D_{hd} \xrightarrow{242.9} I_d$
	8	$K_1 \underset{49.3\ (4.1)}{\overset{64.6\ (5.4)}{\rightleftharpoons}} K_2 \underset{101.2\ (13.4)}{\overset{129.3\ (14.1)}{\rightleftharpoons}} D_{hd} \xrightarrow{236.9} I_d$
	10	$K_1 \xrightarrow{78.2} K_2 \underset{59.3\ (9.1)}{\overset{101.8\ (9.5)^b}{\rightleftharpoons}} D_{hd} \underset{217.3\ (0.6)}{\overset{219.8\ (0.8)}{\rightleftharpoons}} I$
	12	$K_1 \underset{42.1}{\overset{84.6}{\rightleftharpoons}} K_2 \underset{63.1\ (13.4)}{\overset{95.2\ (13.9)^b}{\rightleftharpoons}} D_{hd} \underset{203.6\ (0.9)}{\overset{204.8\ (1.0)}{\rightleftharpoons}} I$
	14	$K_1 \xrightarrow{52.9} K_2 \underset{76.3\ (19.4)}{\overset{88.1\ (18.9)^b}{\rightleftharpoons}} D_{hd} \underset{192.1\ (0.5)}{\overset{192.3\ (0.6)}{\rightleftharpoons}} I$
	16	$K \underset{59.7\ (27.7)}{\overset{91.5\ (24.6)}{\rightleftharpoons}} D_{hd} \underset{176.1\ (0.4)}{\overset{177.7\ (0.4)}{\rightleftharpoons}} I$
2b	10	$K \underset{118.9\ (5.2)}{\overset{156.1\ (3.9)}{\rightleftharpoons}} D_{hd} \xrightarrow{221.5} I_d$
	14	$K \underset{103.7\ (2.9)}{\overset{122.8\ (3.5)}{\rightleftharpoons}} D_{hd} \underset{199.4\ (0.3)}{\overset{205.3\ (0.3)}{\rightleftharpoons}} I$
2c	16	$K_1 \xrightarrow{69.4\ (10.6)} K_2 \underset{61.3\ (10.7)}{\overset{143.0\ (4.1)}{\rightleftharpoons}} K_3 \underset{124.7\ (12.8)^b}{\overset{151.6}{\rightleftharpoons}} K_4 \underset{131.9}{\overset{158.9\ (15.9)^b}{\rightleftharpoons}} I$

[a] All labels and details are as described for Table 1. [b] Combined integrals of broad peaks which overlap with the previous transition.

liquid crystal-to-isotropic (clearing) transition enthalpies range from 0.5 to 2.3 kcal/mol, a relatively small value considering the large molecular weights. The clearing transition temperatures decrease with increasing side-chain length, and the **1a** $n = 8$ and $n = 10$ compounds exhibit the largest range of mesomorphism at about 110°.

Series **1a** with 12 side chains exhibits two mesophase types as shown in Figure 4. The feature controlling the nature of the mesophase is the side-chain length; complexes with shorter side chains ($n \leq 10$) display one type of mesophase and those with longer side chains ($n \geq 12$) display a different phase. The initial phase determinations of **1a** ($n \leq 10$) were performed with the aid of a polarizing microscope. For these derivatives, relatively rapid cooling of the isotropic phase (5 °C/min or faster) produces mosaic regions with wedge shaped defects (plate 1, Figure 5). Additional textures from thin preparations and slow cooling (2 °C/min) exhibited interesting spiral defect patterns (plate 2, Figure 5). In these defect structures the extinction brushes have at 90° separations, and the column axes are arranged in concentric spirals. The column axes are nearly parallel to the glass slides, and these defects can be used to determine the orientation of the molecules relative to the column axes.[25] In the spiral defects of **1a** $n = 6$ extinction is observed at angles of approximately +22° or −22° (plate 2) relative to the analyzer and polarizer directions. From these results it can be concluded that

(24) For reviews on discotics see: (a) Destrade, C.; Foucher, P.; Gasparoux, H.; Nguyen H. T.; Levelut, A. M.; Malthete, J. *Mol. Cryst. Liq. Cryst.* **1984**, *106*, 121. (b) Billard, J. In *Liquid Crystals of One- and Two-Dimensional Order*; Springer Series in Chemical Physics, Berlin, 1980; p 383. (c) Chandrasekhar, S.; Ranganath, G. S. *Rep. Prog. Phys.* **1990**, *53*, 57 and references therein.

(25) Similar analysis of the tilt angle has been reported. Chandrasekhar, S. In *Advances in Liquid Crystals*; Brown, G. H., Ed.; Academic Press: New York, 1982; Vol. 5, p 47.

Table 3. Phase Behavior of Complexes of 3 and 7 (All Labels and Details As Described for Table 1)

compound	n	phase behavior
3a	6	$K_1 \underset{109.5\ (4.2)}{\overset{128.9}{\rightleftharpoons}} K_2 \underset{119.9\ (3.2)}{\overset{131.5\ (8.3)^a}{\rightleftharpoons}} D_{hd} \xrightarrow{245} I_d$
	7	$K_1 \xrightarrow{83.2\ (0.4)} K_2 \underset{95.9\ (4.0)}{\overset{113.9\ (3.9)}{\rightleftharpoons}} D_{hd} \xrightarrow{253} I_d$
	8	$K \underset{76.4\ (6.5)}{\overset{96.1\ (6.4)}{\rightleftharpoons}} D_{hd} \xrightarrow{248} I_d$
	10	$K \underset{54.0\ (4.4)}{\overset{80.9\ (4.9)}{\rightleftharpoons}} D_{hd} \xrightarrow{245} I_d$
	12	$K_1 \underset{34.7\ (4.0)}{\overset{37.8\ (4.5)}{\rightleftharpoons}} K_2 \underset{62.5\ (4.6)}{\overset{81.0\ (5.0)}{\rightleftharpoons}} D_{hd} \xrightarrow{237} I_d$
	14	$K_1 \underset{46.5\ (13.1)}{\overset{66.0\ (10.2)}{\rightleftharpoons}} K_2 \underset{58.0\ (5.2)}{\overset{81.1\ (5.6)}{\rightleftharpoons}} D_{hd} \xrightarrow{248} I_d$
	16	$K_1 \xleftarrow[56.1\ (14.7)^b]{} K_2 \underset{59.4}{\overset{76.0\ (13.1)}{\rightleftharpoons}} D_{hd} \underset{203.8\ (0.6)}{\overset{205.4\ (0.6)}{\rightleftharpoons}} I$
3b	6	$K_1 \underset{39.8\ (2.5)}{\overset{59.8\ (2.9)}{\rightleftharpoons}} K_2 \underset{171.2\ (2.7)}{\overset{182.7\ (3.0)}{\rightleftharpoons}} D_{hd} \xrightarrow{246} I_d$
	7	$K_1 \underset{33.7\ (3.2)}{\overset{63.2\ (2.8)}{\rightleftharpoons}} K_2 \underset{139.8\ (2.2)}{\overset{150.3\ (2.4)}{\rightleftharpoons}} D_{hd} \xrightarrow{244} I_d$
	8	$K_1 \underset{39.3\ (5.3)}{\overset{56.3\ (5.8)}{\rightleftharpoons}} K_2 \underset{80.0\ (0.5)}{\overset{108.4\ (0.6)}{\rightleftharpoons}} D_{hd} \xrightarrow{203} I_d$
	10	$K_1 \underset{30.5\ (6.8)}{\overset{40.3\ (9.4)}{\rightleftharpoons}} K_2 \underset{38.7\ (0.2)}{\overset{60.4\ (0.6)}{\rightleftharpoons}} D_{hd} \xrightarrow{230} I_d$
	12	$K \underset{34.8\ (18.2)}{\overset{52.4\ (18.4)}{\rightleftharpoons}} D_{hd} \xrightarrow{228} I_d$
	14	$K_1 \xrightarrow{54.8} K_2 \underset{30.3\ (12.8)}{\overset{63.9\ (12.4)^a}{\rightleftharpoons}} D_{hd} \underset{197.1\ (0.6)}{\overset{200.1\ (0.6)}{\rightleftharpoons}} I$
3c	12	$K_1 \underset{44.8\ (2.3)}{\overset{77.7\ (0.9)}{\rightleftharpoons}} K_2 \underset{72.7\ (4.3)}{\overset{102.4\ (4.0)}{\rightleftharpoons}} I$
3d	12	$K \underset{121.3\ (14.7)}{\overset{130.3\ (15.3)}{\rightleftharpoons}} I$
3e	12	$K \underset{54.3\ (10.9)}{\overset{85.6\ (12.6)}{\rightleftharpoons}} I$
7a	14	$K \underset{78.8\ (4.2)}{\overset{96.6\ (4.5)}{\rightleftharpoons}} D_{hd} \xrightarrow{226.4} I_d$
	16	$K \underset{67.3\ (2.6)}{\overset{81.6\ (2.7)}{\rightleftharpoons}} D_{hd} \xrightarrow[173.2\ (0.1)]{177.3\ (0.1)} I_d$
7b	14	$K \underset{83.2\ (6.9)}{\overset{105.3\ (6.8)}{\rightleftharpoons}} D_{hd} \xrightarrow{232.4} I_d$
7c	14	$K \xrightarrow{48.3\ (9.6)} I_1 \xrightarrow[-\mathrm{MeOH}]{74} I_2$
7d	14	$K \xrightarrow{50.4\ (12.7)} I_1 \xrightarrow[-\mathrm{MeOH}]{75} I_2$
7e	14	$K \xrightarrow{43.3\ (8.5)} I_1 \xrightarrow[-\mathrm{MeOH}]{74} I_2$

[a] Combined integrals of broad peaks which overlap with the previous transition.

the molecular planes of **1a** $n = 6$ are tilted at ≈22° from the column normal. Similar analysis was possible for the $n = 7$ derivative, and a tilt angle of ≈20° was obtained. Some of these defect patterns display arcs with periodic alternation of the interference colors and a zigzag pattern in some of the extinction brushes (plate 3, Figure 5) which indicates that the orientation of the column axes undulates.

From these optical results and miscibility studies, it can be concluded that **1a** with $n \leq 10$ exhibits a mesophase with a tilted columnar superstructure. Further structural assignment required X-ray diffraction (XRD), and these mesophases display two strong sharp low-angle reflections (Table 5) which transform into a single broad peak in the isotropic phase. The strong low angle peaks are due to well-defined intercolumnar organizations, and higher harmonics of these correlations are observed at slightly higher angles. At wide angle, a single halo is observed which is centered at ≈4.4 Å indicating that all short-range correlations are liquidlike in nature. The number of higher harmonic reflections are sufficient to assign this mesophase more precisely as D_{rd}, thereby indicating that the columns organize in a rectangular superstructure with liquidlike correlations between the molecules within the columns. As shown in Table 5, the strong low-angle peaks are indexed as (200) and (110) and the weaker higher harmonics at slightly higher angles are indexed as (310) and (020). The lattice parameters increase from a = 46.42 Å and b = 22.99 Å for the shortest homologue (n = 5) to a maximum of a = 55.60 Å and b = 30.36 Å for

Table 4. Phase Behavior of Complexes of 4–6[a]

compound	n	phase behavior of complexes
4	6	$K \underset{34.5\ (7.3)}{\overset{65.7\ (7.6)}{\rightleftharpoons}} D_{hd} \underset{200.60\ (0.3)}{\overset{205.89\ (0.3)}{\rightleftharpoons}} I$
	10	$K \underset{80.15\ (9.3)}{\overset{125.53\ (9.4)}{\rightleftharpoons}} D_{hd} \underset{190.72\ (0.6)}{\overset{193.4\ (0.6)}{\rightleftharpoons}} I$
	12	$K \underset{47.29\ (7.3)}{\overset{74.34\ (7.9)}{\rightleftharpoons}} D_{hd} \underset{154.3\ (0.5)}{\overset{159.3\ (0.5)}{\rightleftharpoons}} I$
5a	12	$K \underset{46.7\ (12.4)}{\overset{57.0\ (12.8)}{\rightleftharpoons}} D_{hd} \underset{162.7\ (0.7)}{\overset{165.42\ (0.7)}{\rightleftharpoons}} I$
5b	12	$K \underset{151.7\ (7.9)}{\overset{173.4\ (8.4)}{\rightleftharpoons}} I$
6	12	$K \underset{43.6\ (10.2)}{\overset{61.28\ (10.4)}{\rightleftharpoons}} D_{hd} \underset{170.6\ (0.6)}{\overset{173.512\ (0.6)}{\rightleftharpoons}} I$

[a] All labels and details are as described for Table 1.

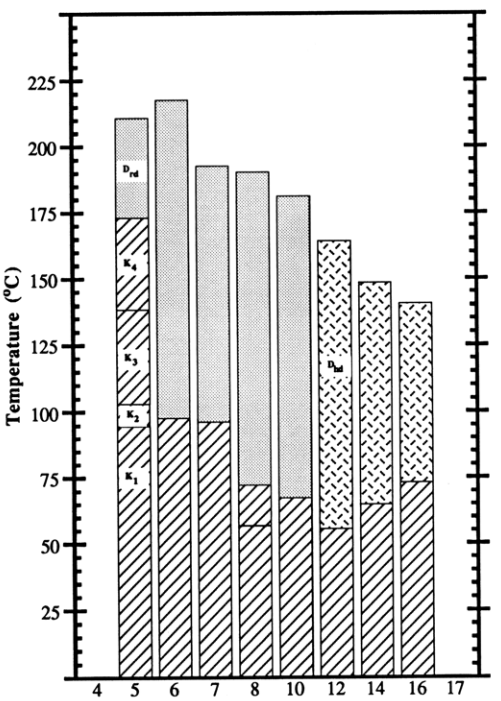

Figure 4. Bar graph showing the phase behavior of **1a**. Similarly shaded areas indicate a similar phase. K1, K2, K3, and K4 indicate different crystal phases, and n is the number of carbon atoms in the side chain.

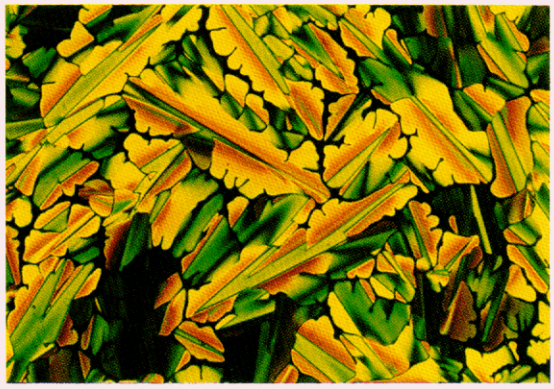

Plate 1

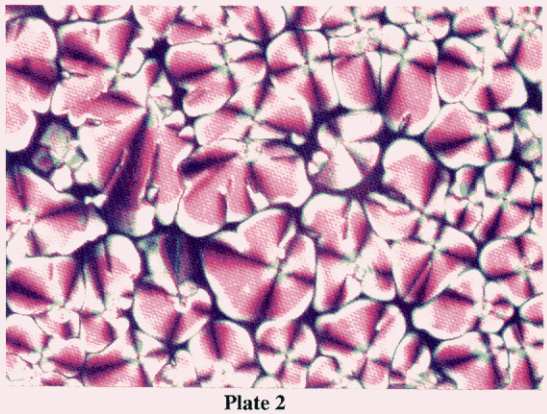

Plate 2

Plate 3

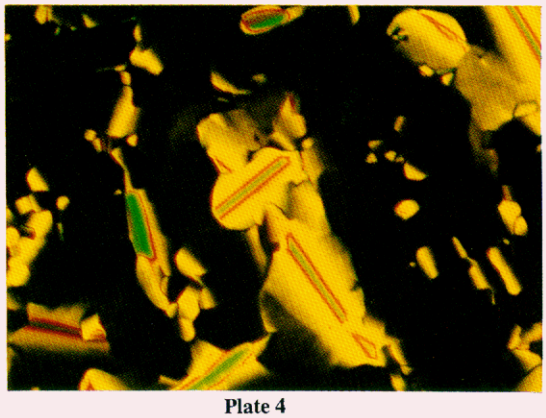

Plate 4

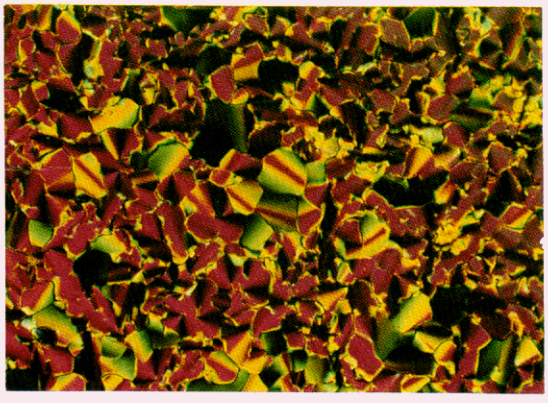

Plate 5

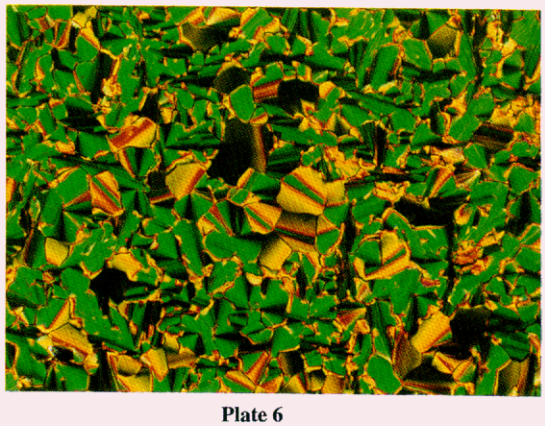

Plate 6

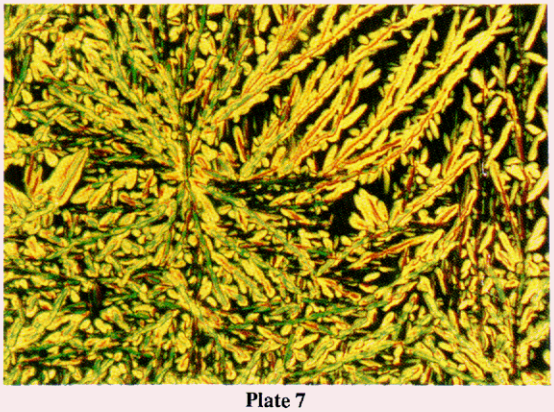

Plate 7

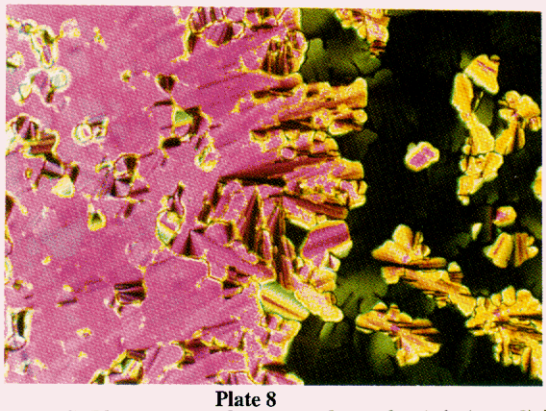

Plate 8

Figure 5. Plate 1: mosaic texture shown by **1a**'s ($n = 6$) D_{rd} phase at 162 °C. Plate 2: spiral texture shown by **1a**'s ($n = 6$) D_{rd} phase at 183 °C. Plate 3: D_{rd} phase of **1a**'s ($n = 6$) at 170 °C. Plate 4: texture exhibited by **1a**'s ($n = 12$) D_{hd} at 144 °C. Plate 5: textures exhibited by the D_{hd} phase of **2a** ($n = 16$) at 60 °C. Plate 6: the K phase of **2a** ($n = 16$) at 55 °C (same region as plate 5). Plate 7: texture shown by **3b**'s ($n = 14$) D_{hd} phase at 153 °C. Plate 8: texture between a contact preparation at 147 °C showing the lack of miscibility of the D_{hd} phase of **2a** ($n = 16$) (left) and **3a**'s ($n = 16$) D_{hd} phase (right). Polarizers are oriented vertical and horizontal.

Table 5. Variable-Temperature XRD Data for Series 1

compound	mesophase	lattice constant, Å	spacing obsd (calcd), Å	Miller indices
1a				
$n = 5$	D_{rd} $C(2/m)$ at 190 °C	$a = 46.42$	23.71 (23.71)	(200)
		$b = 22.99$	19.95 (19.95)	(110)
			12.20 (12.22)	(310)
			11.52 (11.50)	(020)
			4.39	
$n = 6$	D_{rd} $C(2/m)$ at 190 °C	$a = 49.06$	24.53 (24.53)	(200)
		$b = 22.27$	20.28 (20.28)	(110)
			13.17 (13.18)	(310)
			11.14 (11.14)	(020)
			4.38	
$n = 7$	D_{rd} $C(2/m)$ at 190 °C	$a = 52.26$	26.13 (26.13)	(200)
		$b = 26.04$	23.31 (23.31)	(110)
			14.49 (14.49)	(310)
			13.02 (13.02)	(020)
			4.40	
$n = 8$	D_{rd} $C(2/m)$ at 175 °C	$a = 57.00$	28.50 (28.50)	(200)
		$b = 27.10$	24.27 (24.27)	(110)
			15.56 (15.56)	(310)
			12.25 (12.24)	(020)
			4.41	
$n = 10$	D_{rd} $C(2/m)$ at 150 °C	$a = 55.60$	27.80 (27.80)	(200)
		$b = 30.31$	26.61 (26.61)	(110)
			15.79 (15.81)	(310)
			15.15 (15.15)	(020)
			4.44	
$n = 12$	D_{hd} at 150 °C	$a = 33.44$	28.96 (28.96)	(100)
			16.70 (16.70)	(110)
			14.47 (14.48)	(200)
			4.58	
$n = 14$	D_{hd} at 150 °C	$a = 35.84$	31.04 (31.04)	(100)
			17.87 (17.92)	(110)
			15.46 (15.52)	(200)
			4.59	
$n = 16$	D_{hd} at 135 °C	$a = 37.51$	32.48 (32.48)	(100)
			18.76 (18.75)	(110)
			16.24 (16.24)	(200)
			4.58	
1b				
$n = 10$	D_{hd} at 170 °C	$a = 32.27$	27.95 (27.95)	(100)
			16.18 (16.14)	(110)
			13.95 (13.98)	(200)
			4.56	
			3.39	
1c				
$n = 7$	D_{hd} at 190 °C	$a = 28.32$	24.53 (24.53)	(100)
			14.13 (14.16)	(110)
			12.19 (12.26)	(200)
			4.59	
			3.37	
$n = 10$	D_{hd} at 175 °C	$a = 32.26$	27.93 (27.93)	(100)
			16.12 (16.13)	(110)
			13.93 (13.95)	(200)
			4.55	
			3.39	
$n = 16$	D_{hd} at 175 °C	$a = 36.66$	31.75 (31.75)	(100)
			18.25 (18.33)	(110)
			15.90 (15.88)	(200)
			4.55	
			3.38	

the $n = 10$ homologue. We can further assign the symmetry of the D_{rd} phase as ($C_{2/m}$), since ($P2/a$) is excluded due to the absence of the (210) Bragg peak, and on the basis of the molecular size we can discount the possibility of ($P2_1/b$) symmetry.[26] As shown in Figure 3, the molecules in this symmetry of rectangular superstructure all tilt in the same direction, and such an arrangement is also consistent with our optical analysis. The ratio of a/b indicates that the shorter side-chain homologues exhibit a greater anisotropy (i.e., more elliptical) along the columnar axis than the longer side-chain homologues. This greater anisotropy results from the higher core to side-chain ratio, since although the cores are tilted, the side chains are free to extend radially at right angles to the column's axis.

Complexes **1a** with ($n \geq 12$) and derivatives **1b** and **1c** all display the same type of mesophase which is totally immiscible with the D_{rd} phase just discussed. The reduced side-chain density in compounds **1b** and **1c** relative to their homologues in series **1a** results in an increase in both the crystal-to-mesophase and mesophase-to-isotropic transition temperatures. Complexes **1c** exhibit relatively high clearing points (ca. 190–250 °C) which for $n \leq 10$ are accompanied by decomposition. Slow cooling (2 °C/min) of **1a**'s ($n \geq 12$) isotropic phase reveal mesophase textures displaying digitated star domains which are visible in the optical microscope without the use of polarizers. These patterns initially display little or no birefringence, and continued cooling produces coalesced domains with areas of uniform extinction interspersed with regions displaying linear birefringent defects and leaflike patterns (plate 4, Figure 5). The large fraction of regions lacking birefringence indicates that these materials are optically uniaxial and that the optic axis readily aligns normal to the glass microscope slides. These features and the presence of the linear birefringent defects indicates conclusively that these phases have a hexagonal or close packed columnar superstructure (D_{hd}) in which the average orientation of the molecular planes is perpendicular to the column's axis. The XRD data are also characteristic of a D_{hd} phase, displaying one intense and two weak low-angle peaks with a d-spacing ratio of $1:(1/3)^{1/2}:1/2$. These peaks correspond to the (100), (110), and (200) Bragg peaks of a hexagonal lattice, respectively (Table 5). At wide angle, all the **1a** homologues display a single halo centered at ≈4.6 Å which corresponds to liquidlike correlations between the alkyl chains and the mesogenic cores. Compounds **1b** and **1c** display a halo at ≈4.6 Å but have an additional broad peak at 3.37–3.39 Å. The former is a result of the correlations between alkyl chains, while the latter indicates these materials exhibit a closer and slightly more regular packing of the mesogenic cores than observed for **1a**.

Compounds **2a** and **2b** which contain six alkyloxy side chains were found to display liquid crystallinity with low isotropic transition enthalpies (0.3–1.0 kcal/mol) as shown in Table 2. Decreasing the number of side chains to four for **2c** gives only crystal-to-crystal and crystal-to-isotropic phase transitions with large (15.9 kcal/mol) isotropic transition enthalpies. Compounds **2a** and **2b** exhibit relatively high clearing points ranging from 178 °C for the longest side-chain derivatives ($n = 16$) to 265 °C for the shortest side-chain derivatives ($n = 5$, Figure 6). Due to these high temperatures, compounds with $n < 10$ decompose in their isotropic melts. The crystal-to-mesophase transition temperature is also reduced with side-chain length, and the width of mesomorphism ranges from 85 to 110 °C throughout the homologous series. The electronic induction of the CF_3 moiety in **2b** results in greater intermolecular associations, and the melting transition raises relative to the corresponding **2a** homologues by 55 and 34 °C for $n = 10$ and 14, respectively. The CF_3 substitution also effects the

(26) (a) Cook, M. J.; Mckeown, N. B.; Thomson, A. J.; Harrison, K. J.; Richardson, R. M.; Davies, A. N.; Soser, S. J. *Chem. Mater.* **1989**, *1*, 287. (b) Ohta, K.; Takeenaka, O.; Hasebe, H.; Morizumi, Y.; Fujimoto, T.; Yamamoto, I. *Mol. Cryst. Liq. Cryst.* **1991**, *195*, 135.

Table 6. Variable-Temperature XRD Data of Series 2a and 2b

compound	mesophase	lattice constant, Å	spacing obsd (calcd), Å	Miller indices
2a				
$n = 5$	D_{hd} at 190 °C	$a = 24.86$	21.53 (21.53)	(100)
			12.48 (12.43)	(110)
			10.85 (10.77)	(200)
			4.58	
			3.29	
$n = 6$	D_{hd} at 190 °C	$a = 25.78$	22.33 (22.33)	(100)
			12.89 (12.89)	(110)
			11.10 (11.16)	(200)
			4.55	
			3.29	
$n = 7$	D_{hd} at 190 °C	$a = 26.92$	23.31 (23.31)	(100)
			13.40 (13.46)	(110)
			11.51 (11.66)	(200)
			4.55	
			3.30	
$n = 8$	D_{hd} at 175 °C	$a = 27.61$	23.91 (23.91)	(100)
			13.73 (13.80)	(110)
			11.91 (11.96)	(200)
			4.58	
			3.31	
$n = 10$	D_{hd} at 150 °C	$a = 30.46$	26.38 (26.38)	(100)
			15.20 (15.23)	(110)
			13.18 (13.19)	(200)
			4.58	
			3.31	
$n = 12$	D_{hd} at 150 °C	$a = 32.60$	28.23 (28.23)	(100)
			16.30 (16.30)	(110)
			14.15 (14.12)	(200)
			4.55	
			3.31	
$n = 14$	D_{hd} at 150 °C	$a = 35.06$	30.36 (30.36)	(100)
			17.53 (17.53)	(110)
			15.21 (15.18)	(200)
			4.55	
			3.30	
$n = 16$	D_{hd} at 135 °C	$a = 35.84$	31.04 (31.04)	(100)
			17.92 (17.92)	(110)
			15.51 (15.52)	(200)
			4.56	
			3.31	
2b				
$n = 10$	D_{hd} at 170 °C	$a = 31.04$	26.88 (26.88)	(100)
			16.43 (15.52)	(110)
			13.38 (13.44)	(200)
			4.58	
			3.29	
$n = 14$	D_{hd} at 190 °C	$a = 35.26$	31.04 (30.54)	(100)
			17.89 (17.63)	(110)
			15.51 (15.77)	(200)
			4.55	
			3.29	

isotropic transition but to a lesser degree, and **2b** $n = 10$ and $n = 14$ exhibit respective clearing points that are 2° and 13° higher than the corresponding **2a** homologues. Optical microscopy and miscibility studies indicate that **2a** and **2b** exhibit the same mesophase. Optical textures for **2a** and **2b** produced by slow cooling (2 °C/min) from their isotropic phases are a mixture of pseudo-focal conic fans and mosaic regions with linear birefringent defects (plate 5, Figure 5) suggestive of a hexagonal columnar structure (D_{hd}). X-ray diffraction (Table 6) confirmed our optical results, and the D_{hd} phase of **2a** and **2b** showed (100), (110), and (200) Bragg peaks in the ratio $1:(1/3)^{1/2}:1/2$ and halos at 4.55–4.58 and a peak at 3.29–3.31 Å. It is noteworthy that the halo at ≈3.3 Å for **2a** and **2b** has a smaller d spacing, is sharper, and is more intense than those observed for **1b** and **1c** indicating a tighter registry of molecules within the columns. The interference colors exhibited by **2a** under the polarizing microscope display a large increase in birefringence upon cooling into the crystal phase (plate 6, Figure 5). This abrupt change occurs without the introduction of new defects, indicating that the crystal phase does not involve a dramatic reorganization of the mesogenic cores. The crystal phase has a lamellar structure as we observes six orders of diffraction which index to a single periodicity. The change in birefringence is paralleled by shifts of the 1,3,5-triketonate's C=C and C=O stretching frequencies. Particularly important is the change in the C=C stretching band which shifts from 1560 to 1500 cm^{-1} at the crystal phase transition. Although the changes in the infrared spectrum cannot be used for definitive structural assignments, it seems likely that the spectral and birefringence changes are the result of the conformational dynamics the phenyl groups.[27] Hence, a static and more conjugated planar conformation of the phenyl groups in the crystal phase is consistent with an increase in birefringence and a shift in the C=C to lower energy. In contrast, **2b**'s texture showed no change in its birefringence upon entering the crystal phase, and consistent with this result, infrared analysis reveals that the bands of the triketonate are insensitive to phase transitions.

The area of **3**'s mesogenic cores are nearly identical to those of series **2**, and again the four side-chain derivative **3c** is not liquid crystalline, whereas the six side-chain complexes **3a** and **3b** are mesomorphic. The sterically encumbering linkages between the Schiff bases in complexes **3d** and **3e** reduce the intermolecular attractive interactions sufficiently to eliminate liquid crystallinity. Complexes **3a** and **3b** exhibit relatively high clearing points 200–253 °C, and again the shorter side-chain analogues lie at the upper limits of this range and decompose in their isotropic phase. The longer side chains ($n \geq 14$) display stable isotropic phases with small clearing enthalpies of 0.6 kcal/mol. The melting transitions ranged from 60 to 183 °C (ΔH_{melt} = 5–20 kcal/mol), yielding mesomorphic ranges of 70–170 °C with the longer side-chain complexes displaying wider phase stability (Table 3). The optical textures of **3a** and **3b** are characteristic of a D_{hd} phase. Compound **3a** tends to produce textures with mosaic domains with linear birefringent defects, while **3b**'s textures are generally dominated by digitized contours and leaflike patterns enveloped in large regions of uniform extinction (plate 7, Figure 5). The X-ray diffraction patterns from the D_{hd} phases of **3a** and **3b** (Table 7) were nearly indistinguishable from those of **2a**. We find that the (100), (110), and (200) Bragg peaks have nearly identical positions and relative intensities to their **2a** homologues, and the halos at 4.6 and the peaks at 3.30–3.32 Å are also very similar. Despite all of the similarities between **2** and **3**, their D_{hd} phases are not miscible (plate 8, Figure 5) suggesting a more complex organization within the mesophase than typically exhibited for discotics. The textures of **3a** and **3b** showed very minimal change in birefringence upon entering the crystal phase, suggesting that the molecular conformation does not change dramatically. However, infrared spectra show the C=N stretching band to shift from 1522 cm^{-1} in the mesophase to 1507 cm^{-1} in the crystal

(27) We have previously seen this type of behavior in metal diketonate complexes: Zheng, H.; Swager, T. M. *J. Am. Chem. Soc.* **1994**, *116*, 761.

Table 7. Variable-Temperature XRD Data for 3a, 3b, 7a, and 7b

compound	mesophase	lattice constant, Å	spacing obsd (calcd), Å	Miller indices
3a				
$n = 6$	D_{hd} at 170 °C	$a = 25.65$	22.21 (22.21)	(100)
			13.82 (13.82)	(110)
			11.10 (11.11)	(200)
			4.56	
			3.32	
$n = 7$	D_{hd} at 170 °C	$a = 26.05$	22.56 (22.56)	(100)
			13.02 (13.03)	(110)
			11.25 (11.28)	(200)
			4.60	
			3.32	
$n = 8$	D_{hd} at 170 °C	$a = 27.38$	23.71 (23.71)	(100)
			13.73 (13.69)	(110)
			11.82 (11.86)	(200)
			4.56	
			3.31	
$n = 10$	D_{hd} at 170 °C	$a = 30.14$	26.10 (26.10)	(100)
			15.05 (15.07)	(110)
			13.04 (13.05)	(200)
			4.56	
			3.31	
$n = 12$	D_{hd} at 170 °C	$a = 32.27$	27.95 (27.95)	(100)
			16.13 (16.14)	(110)
			14.01 (13.98)	(200)
			4.58	
			3.32	
$n = 14$	D_{hd} at 160 °C	$a = 34.14$	29.57 (29.57)	(100)
			17.05 (17.07)	(110)
			14.76 (14.79)	(200)
			4.55	
			3.31	
$n = 16$	D_{hd} at 120 °C	$a = 35.06$	30.36 (30.36)	(100)
			17.53 (17.53)	(110)
			15.17 (15.18)	(200)
			4.58	
			3.32	
3b				
$n = 6$	D_{hd} at 170 °C	$a = 25.38$	21.98 (21.98)	(100)
			12.73 (12.69)	(110)
			11.00 (10.99)	(200)
			4.55	
			3.29	
$n = 7$	D_{hd} at 190 °C	$a = 26.07$	22.58 (22.58)	(100)
			13.06 (13.04)	(110)
			11.31 (11.29)	(200)
			4.55	
			3.32	
$n = 8$	D_{hd} at 170 °C	$a = 27.68$	23.97 (23.97)	(100)
			13.82 (13.84)	(110)
			11.98 (11.99)	(200)
			4.56	
			3.30	
$n = 10$	D_{hd} at 170 °C	$a = 29.90$	29.90 (29.90)	(100)
			14.88 (14.95)	(110)
			12.93 (12.95)	(200)
			4.55	
			3.32	
$n = 12$	D_{hd} at 170 °C	$a = 32.27$	27.95 (27.95)	(100)
			16.11 (16.14)	(110)
			13.94 (13.98)	(200)
			4.55	
			3.30	
$n = 14$	D_{hd} at 190 °C	$a = 34.33$	29.73 (29.73)	(100)
			17.16 (17.16)	(110)
			14.80 (14.87)	(200)
			4.58	
			3.29	
7a				
$n = 14$	D_{hd} at 140 °C	$a = 34.35$	29.75 (29.75)	(100)
			17.21 (17.18)	(110)
			14.83 (14.88)	(200)
			4.56	
			3.31	
$n = 16$	D_{hd} at 120 °C	$a = 35.41$	30.67 (30.67)	(100)
			17.70 (17.71)	(110)
			15.32 (15.34)	(200)
			4.58	
			3.30	
7b				
$n = 14$	D_{hd} at 160 °C	$a = 34.58$	29.95 (29.95)	(100)
			17.24 (17.29)	(110)
			14.90 (14.98)	(200)
			4.58	
			3.31	

Table 8. Variable-Temperature XRD Data for 4, 5a, and 6

compound	mesophase	lattice constant, Å	spacing obsd (calcd), Å	Miller indices
4				
$n = 6$	D_{hd} at 175 °C	$a = 27.43$	23.76 (23.76)	(100)
			13.70 (13.72)	(110)
			4.58	
$n = 10$	D_{hd} at 140 °C	$a = 32.60$	28.23 (28.23)	(100)
			16.29 (16.30)	(110)
			14.06 (14.12)	(200)
			4.60	
$n = 12$	D_{hd} at 80 °C	$a = 34.03$	29.47 (29.08)	(100)
			16.92 (17.01)	(110)
			14.63 (14.74)	(200)
			4.58	
5a				
$n = 12$	D_{hd} at 80 °C	$a = 33.61$	29.11 (29.11)	(100)
			16.67 (16.81)	(110)
			14.56 (14.59)	(200)
			4.56	
6				
$n = 12$	D_{hd} at 90 °C	$a = 33.52$	29.03 (29.03)	(100)
			16.70 (16.76)	(110)
			14.38 (14.52)	(200)
			4.55	

phase. This effect may be an indirect result of intermolecular Cu—O dative bonding.

The tetraketonate derivatives **4**, **5a**, and **6** display wide ranges of mesomorphism (68−140°, Table 4) and lower mesophase-to-isotropic transition enthalpies of 0.3−0.7 kcal/mol that are lower than their triketonate relatives. In addition, the tetraketonates are qualitatively more fluid in their liquid-crystalline phases than the triketonates. Despite their larger core, the clearing and melting transitions of the tetraketonates tend to be lower that the related triketonates. The clearing transitions of **4** are reduced slightly (5−11°) from their **1a** homologues. However, more dramatic reductions are found for **5a** and **6** in which the isotropic transitions are reduced by 40° and 64° from their **2a** and **3a** homologues, respectively. The structural similarities with the triketonates are reflected in the phase behavior, and the four-side-chain derivative **5b** is not mesogenic while the six-side-chain compounds (**5a** and **6**) are liquid crystalline. Miscibility studies indicate that the tetraketonates **5a** and **6** are miscible with the related triketonates of the same structural type, **2a** and **3a**, respectively, indicating that they exhibit the same D_{hd} mesophases. These phase assignments were also confirmed by optical and XRD studies. Again, as was the case in the triketonates, **5a** and **6** are not miscible with D_{hd}-forming complexes of a different shape. For example, **5a** is not miscible with **3a** or any of the compounds of series **1**. Compounds **4** are miscible with the D_{hd}-forming materials of series **1**, and in contrast to series **1a** the shorter side-chain analogs of **4** do not exhibit a D_{rd} phase. The optical textures of **4**−**6** showed these materials to readily align with their column's axis normal to the glass slides, thereby producing samples with greater than 90% uniform extinction with slow cooling (0.1 °C/min). These textures also displayed small fractions of mosaic regions containing linear birefringent defects. The qualitatively lower viscosity and tendency for homogeneous alignment indicate that these materials exhibit a low interfacial viscosity which allows defects introduced by the interface or by dust particles to heal. X-ray diffraction of the mesophases of **4**−**6** displayed the (100), (110), and (200) Bragg peaks characteristic of the D_{hd} phase and an amorphous halo

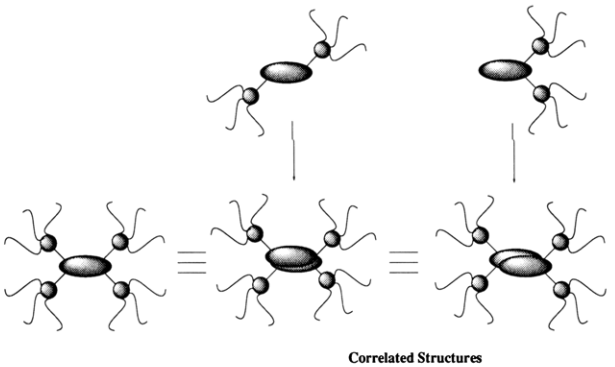

Figure 6. Disk-shaped structures formed by homo- and heteronuclear bimetallic complexes. Compounds **1a** and **4** can approximate a disk-shape in unimolecular form (left). A 90° rotation of nearest neighbors of **2** and **5a** produce a similar disk-shape (center) while **3** and **6** require a 180° rotation of nearest-neighboring molecules (right).

at 4.55–4.60 Å. However, these materials do not display the additional wide angle peak which was observed for series **2** and **3**, indicating weaker correlations between the cores in the columns.

The greater tendency for some members of series **7** to retain coordinated methanol greatly reduces the ability of these heteronuclear compounds to display liquid crystallinity. Compounds **7c–e**, which have axially coordinated methanol, melt directly to an isotropic phase at low temperature (43–50 °C). Further heating resulted in dissociation of methanol at ≈75 °C to produce an additional isotropic phase. The copper and the palladium complexes, **7a** and **7b**, respectively, do not retain methanol and display liquid-crystalline behavior very similar to the homonuclear dicopper complexes with pendant chains of comparable length. They showed relatively high clearing points about 200 °C, which was normally accompanied with decomposition (Table 3). Complex **7a** (n = 16) displays a stable isotropic phase and a transition enthalpy of 0.1 kcal/mol. Compounds **7a** and **7b** exhibit optical textures and XRD patterns very similar to their **3a** homologues.

Complementary Shapes and Superstructure. Most thermotropic columnar phases are based upon discoid molecules which organize as shown in Figure 3.[24] However, while all of the liquid crystals discussed herein display columnar phases, only complexes of series **1** and **4** have structures which can approximate a disk shape. All of the other mesogenic complexes have a hemidisk shape, and their behaviors can be understood only by considering that highly correlated structures are present in the mesophases.[28] Hence, as shown in Figure 6, complexes **2a**, **2b**, and **5** adopt a disk shape through a time-averaged structure with nearest neighbors rotated by 90°. The nearest neighbors of the Schiff-base complexes **3a**, **3b**, **7a**, and **7b** similarly rotate by 180° on time average. It is important to note that these materials are fluids, and the correlated structures shown in Figure 6 are time averaged representations. We refer to the structures having the 180° or antiparallel correlation as "discotic antiphases" in analogy to the smectic antiphases in which polar mesogens exhibit antiparallel correlations.[29]

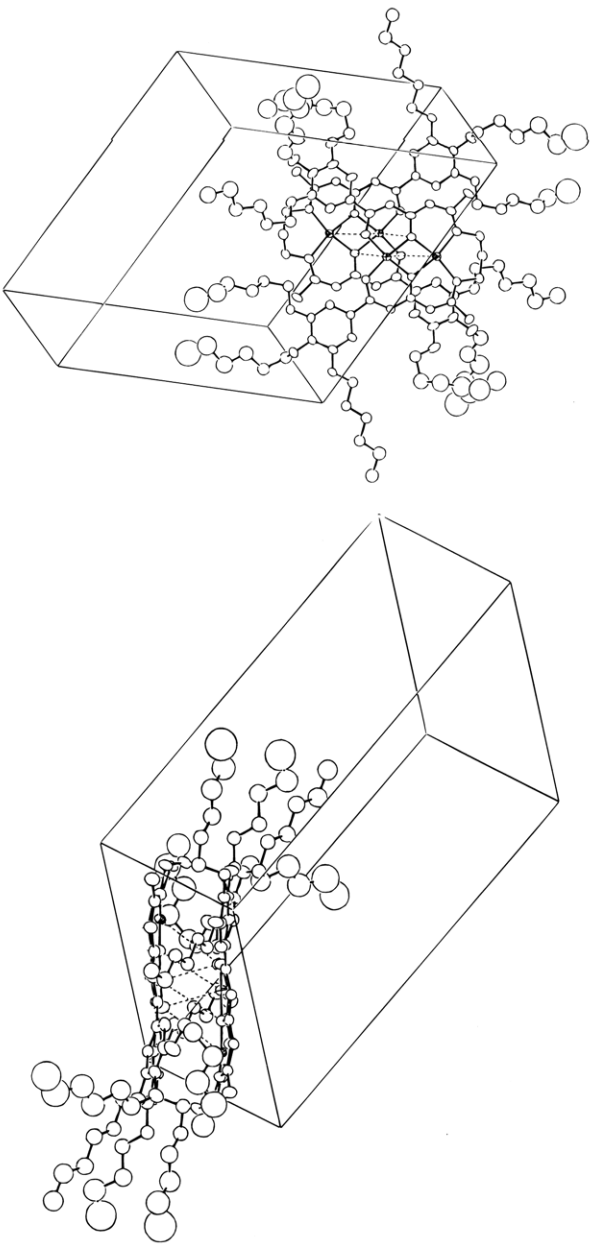

Figure 7. ORTEP (two views) of **3b** (n = 6) with the hydrogens omitted for clarity. The thermal ellipsoids are drawn at 30% and the dative Cu–O interactions are shown as dotted lines.

The Schiff-base compounds also have a tendency to adopt an antiparallel structure in the crystal phase. The crystal structure of **3b** (n = 6, Figure 7) shows that the compounds assemble in a rigorously antiparallel dimeric arrangement. The dimerization of the complexes occurs through intermolecular dative associations between pairs of oxygens and copper centers. The intermolecular dative bonds are 3.66, 3.65, and 3.04 Å in length, and the copper centers are pulled 0.028 and 0.036 Å from the equatorial plane.

(28) Other nondiscoid molecules have been found to display columnar mesomorphism. For reports on hemidiscs see: (a) Barberá, J.; Cativiela, C.; Serrano, J. L.; Zurbano, M. M. *Adv. Mater.* **1991**, *3*, 602. (b) Zheng, H.; Lai, C. K.; Swager, T. M. *Chem. Mater.* **1994**, *6*, 101. For discotic behavior in phasmidic compounds see: (c) Malthéte J.; Levelut, A. M.; Tinh, N. H. *J. Phys. Lett.* **1985**, *46*, L875. (d) Malthéte J.; Tinh, N. H.; Levelut, A. M. *J. Chem. Soc., Chem. Commun.* **1986**, 548. (e) Malthéte J.; Collet, A.; Levelut, A. M. *Liq. Cryst.* **1989**, *5*, 123. For reports of tapered or wedge shaped mesogens see: (f) Pervec, V.; Johansson, G.; Heck, J.; Ungar, G.; Batty, S. V. *J. Chem. Soc., Perkin Trans.* **1993**, 1411. (g) Tomazos, D.; Out, G.; Heck, J. A.; Johansson, G.; Percec, V.; Möller, M. *Liq. Cryst.* **1994**, *16*, 509 and references therein. For a very recent report of columnar mesomorphism in octahedral complexes see ref 27.

(29) Gray, G. W.; Goodby, J. W. G. *Smectic Liquid Crystals; Textures and Structures*; Leonard Hill Publishers: Glasgow, 1984, pp 143–149.

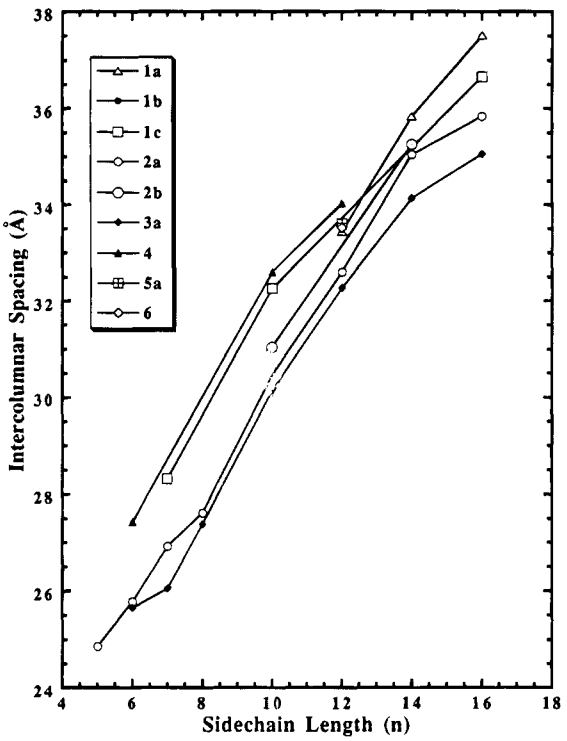

Figure 8. Plot of the intercolumnar spacing (a) vs side-chain length (n) of various D_{hd} phases.

A comparison of the column diameters (a) as a function of side-chain length (n) for all the D_{hd} phases also supports the presence of correlated structures in the mesophases. As shown in Figure 8, all of the compounds of a given side-chain length have surprisingly similar lattice parameter a. For the shorter side chains, the slopes (a, n) are roughly linear and parallel. For the longer side chains (n > 12) the plots are less linear and there is a general trend toward decreasing slopes. The similar slopes suggest that the side-chain density in the columns is similar for all of the materials which results in comparable amounts of side-chain interdigitation for given side-chain lengths. The volume that must be occupied by the side chains scales with the square of the radius, and as a result the volume increases more rapidly at larger a. A reduced slope (a, n) for longer side chains is therefore understood to be the result of incomplete filling of space at the columns perimeter, which leads to greater side-chain interdigitation between neighboring columns. The similarities between all of the compounds emanate from the correlated structures, which allow the mesogens to behave as if they have the same shape. This aspect is particularly apparent in the 12-side-chain tetraketonate complex **4**, which exhibits a lattice spacing only ≈2 Å larger than the six-side-chain triketonate homologues, a variance attributed to the difference of the dimensions of the triketonate and tetraketonate mesogenic cores. The trends from Figure 8 are particularly similar for complexes **2a** and **3a**. Likewise **5a** and **6a** (n = 12) have nearly identical lattice constants. The trends in column size are also consistent with **3b**'s crystal structure. Extrapolation of the linear part of the a vs n plot to n = 0 for **3a** ($n \leq 12$) gives a core diameter of 19.4 Å which is almost identical with the distance across the diagonal of the dimerized complex, measured at 19.2 Å from **3b**'s crystal structure. This also suggests that the organization of these molecules in the liquid-crystalline phase is similar to that in the crystal structure.

From the preceding discussion it is apparent that the bimetallomesogens in this study produce a D_{hd} phase which is relatively insensitive to the number of side chains. The 12-side-chain triketonates are less than 6% larger than their 6-side-chain homologues. The difference is even less in the tetraketonates where **4** (n = 12) is less than 2% larger than **5a** and **6**. To maintain a similar column size, the mesogenic cores with fewer side chains must pack closer together which is apparent in the wide-angle XRD data. For all of the compounds investigated we observe a halo centered at 4.4–4.6 Å which is primarily due to liquidlike correlations between the paraffin side chains. For the 12-side-chain complexes **1a** and **4** this halo is the only peak visible at wide angle, thereby indicating that the correlations between the mesogenic cores also contribute to this halo and that intermesogen correlations are very weak. However, for **1b**, **1c**, **2a**, **2b**, **3a**, **3b**, **7a**, and **7b** which have fewer side chains, we observe an additional broad peak at ≈3.3 Å which indicates stronger and closer correlations between the mesogenic cores. The tighter packing of these mesogenic cores compensates for the fewer side chains and produces a column with a side-chain density at its perimeter which is similar to that of **1a** and **4**. It is noteworthy that the six-side-chain tetraketonate complexes **5a** and **6** display only a single wide angle peak at ≈4.6 Å. We believe that the lack of stronger intermesogen correlations in these materials is due to the greater flexibility of the mesogenic core. This flexibility results in bending and twisting deformations and more fluctuations in the mesophase state which reduce the core–core correlations. Consistent with this explanation is the fact that all of the tetraketonates have lower melting and clearing points than their triketonate homologues and the fact that the tetraketonates have qualitatively greater fluidity in their mesophases.

Intermolecular Associations and Mesophase Stability. A feature key to the stabilization of some phases in metallomesogens is the presence of weak intermolecular bonding.[8] This feature is particularly important for square-planar complexes, and indeed most crystal structures show some bonding interactions at the axial sites. Since all of the liquid-crystalline complexes in this study have two square-planar metal centers, it seems likely that dative associations may play a particularly important role in controlling mesophase stability. In fact, the additional wide-angle XRD peaks for the D_{hd} phases of **1b**, **1c**, **2a**, **2b**, **3a**, **3b**, **7a**, and **7b** indicate an average intermesogen distance of ≈3.3 Å, a distance between the longest and shortest Cu–O dative bonds found in **3b**'s crystal structure. Additionally, the electron-withdrawing nature of **3b**'s CF_3 group increases the ligand affinity of the copper centers thereby increasing intermolecular associations and raising both the melting and clearing temperatures. Hence, it seems likely that all the compounds exhibit varying degrees of dative associations in the mesophase and the crystal phase.

Intermolecular dative associations are often the key to understanding the balance between stability and instability of metal containing liquid-crystalline phases.[8] For example, the steric bulk in the Schiff-base bridging groups of **3d** and **3e** dramatically reduces intermolecular associations, and no liquid crystallinity is observed. Likewise, the presence of coordinated methanol in **7c–e** prevents intermolecular associations and mesomor-

phism. On the other hand, too strong of associations can also prevent liquid crystallinity, as we find that thermal dissociation of the coordinated methanol produces highly associated materials which are also not liquid crystalline. In the case of **7a** and **7b** there is also the possibility that metal−metal interactions may play a role in the stabilization of the mesophase. The presence of the D_{rd} phase for **1a** $n \leq 10$ may also be the result of dative associations. Molecules with shorter side chains are more restricted by axial coordination which is maximized in a tilted D_{rd} structure wherein the molecules exhibit a slight offset as shown here:

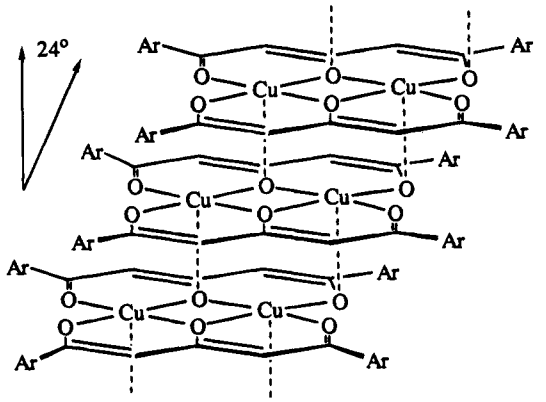

Such a structure has an intermolecular offset similar to what is observed in the X-ray structure of **3b**. A tilt angle can be calculated for this structure using simple geometry[30] to be ≈24°, a value similar to that obtained by optical microscopy. Lengthening the side chains of **1a** to $n \geq 12$ increases the dispersive forces which allow the molecules to rotate more freely, and the D_{hd} becomes more stable. Also consistent with this explanation is the fact that the halo in the D_{rd} phase is observed at 4.4 Å, a value 0.2 Å smaller than that in the D_{hd} phase of **1a** $n \geq 12$, indicating a slightly denser packing of the cores.

Summary and Outlook

We have conducted a detailed study of the mesomorphic properties of triketonate and tetraketonate bimetallomesogens. The first heteronuclear metallomesogens with strongly interacting metal centers were reported. Systematic investigations of a large number (51) of compounds have allowed for a general understanding of the liquid-crystalline properties of these materials. Intermolecular dative coordination interactions were found to stabilize or destroy liquid-crystalline phases, depending upon their strength. Methodology was demonstrated by which polymetallic liquid crystals may be assembled into well-defined columnar superstructures. This methodology makes use of time-averaged correlated structures, and the presence of these correlations was shown through the similarities in the liquid-crystalline properties, liquid-crystalline structure, and comparisons with an X-ray crystal structure. The need for complementary shapes was demonstrated by the immiscibility between materials having the same phase but different shapes. These principles of shape complementarity are general and can be applied to other liquid-crystalline materials, to create organized assemblies with tailored intermolecular interactions. The discotic antiphases of **7a** and **7b** exhibit a structure in which the intermolecular heteronuclear distances are shorter than the homonuclear distances. This positional control of metal centers in polymetallic liquid crystals is critical to develop metallomesogen-based materials with new properties. In addition, the correlated structures produce relatively tight packing of the mesogenic cores while maintaining good mesomorphic properties. XRD indicates a average distance between the mesogenic cores of ≈3.3 Å, which are comparable to the closest intermolecular distances reported for metallomesogens.[31] As a result correlated structures are useful in generating strong intermolecular interactions in a mesomorphic state. An application of the methodologies discussed may be in the design of liquid crystals with ferrimagnetic correlations. In polymeric heteronuclear materials based upon Cu^{2+} and Mn^{2+} shorter heteronuclear contacts have been shown to control the bulk magnetic properties.[32] In addition, the ability to position transition metals relative to one another in liquid crystals has potential applications in the development of sensory and catalytic materials. In future investigations we will focus upon using the principles demonstrated herein to explore the interplay of the molecular superstructure and electrical, optical, and magnetic properties of metal containing liquid crystals.

Experimental Section

General Methods. ^1H and ^{13}C NMR spectra were recorded on a Bruker AC-250. Chemical shifts are reported in ppm relative to residual $CHCl_3$ (δ = 7.24, ^1H; 77.0,^{13}C). Multiplicities are given as s (singlet), d (doublet), t (triplet), q (quartet), m (multiplet), and md (multiplet of doublets). Infrared spectra were recorded using a Perkin-Elmer 1760-X FTIR, and polystyrene was used as a standard. High-resolution FAB mass spectroscopy was performed on a VG analytical ZAB-E instrument using $CHCl_3$ as a solvent with 3-nitrobenzyl alcohol as the matrix. Elemental analysis for carbon, hydrogen, and nitrogen were performed on a Perkin-Elmer 240C elemental analyzer, and all analyses of the metals were performed by Galbraith Laboratories Inc. Optical characterization was performed using covered microscope slides on a Wild Leitz polarizing microscope equipped with a Mettler FP 82 hot stage and a Mettler FP 800 central processor. Variable-temperature infrared spectroscopy was performed by sandwiching a thin film of sample between two 6 mm × 1 mm KBr plates and inserting the plates into the Mettler FP 82 hot stage which was mounting in the IR beam. Transition temperatures and heats of fusion were determined at scan rates of 10 °C min^{-1} by differential scanning calorimetry using a Perkin-Elmer DSC 7 system calorimeter which was calibrated with indium and tin standards in conjunction with a Perkin-Elmer 7700 thermal analysis data station . Variable-temperature X-ray diffraction was measured using Cu Kα radiation on an Inel CPS 120 position-sensitive detector with a XRG 2000 generator, a fine-focus X-ray tube, and a home-built heating stage. The temperature was regulated with a Minco CT 137 temperature controller with ±1 °C temperature stability. Approximately 2 mg samples were suspended in 0.5 mm Lindermann glass capillaries. The detector was calibrated using mica and silicon standards which were obtained from the National Bureau of Standards (NBS).

Unless otherwise indicated, all chemicals and solvents were reagent grade and were used as obtained without further purification. Dimethoxyethane (DME) was distilled from a

(30) The Cu/O offset distance from such an arrangement is calculated to be ≈2.0 Å. Considering an average intermesogen distance of 4.4 Å, the tilt angle is arctan(2.0 Å/4.4 Å) = 24.4°.

(31) Vacus, J.; Doppelt, P.; Simon, J.; Memetzidis, G. *J. Mater. Chem.* **1992**, *2*, 1065.

(32) Kahn, O.; Pei, Y. A.; Verdaguer, M.; Renard, J. P.; Sletten, J. *J. Am. Chem. Soc.* **1988**, *110*, 782.

sodium benzophenone ketyl, and ethyl acetate was predried with 4 Å molecular sieves. Throughout the experimental n represents the number of carbon atoms in the alkyl chain. Fractional peaks due to tautomers are given in brackets.

Platelike crystals suitable for an X-ray diffraction experiment were obtained by slow diffusion of acetone into a THF solution of **3b** ($n = 6$) at 0 °C. The crystals studied were glued on a glass fiber and mounted on a Enraf-Nonius CAD4 diffractometer. The cell constants were determined from a least-squares fit of the setting angles for 25 accurately centered reflections. X-ray intensity data were collected on an Enraf-Nonius CAD4 diffractometer employing graphite-monochromated Mo Kα radiation ($\lambda = 0.710\ 73$ Å) and using the $\omega-2\theta$ scan technique. A total of 15741 reflections were measured over the ranges $4 \le 2\theta \le 55°$, $0 \le h \le 11$, $-23 \le k \le 23$, $-27 \le l \le 27$. Three standard reflections measured every 3500 s of X-ray exposure showed no intensity decay over the course of data collection.

The intensity data were corrected for Lorentz and polarization effects and an empirical absorption correction was applied. Of the reflections measured a total of 8268 unique reflections with $F^2 > 3\sigma(F^2)$ were used during subsequent structure refinement.

The structure was solved by standard heavy-atom Patterson techniques followed by weighted Fourier syntheses. Refinement was by the full-matrix least-squares techniques based on F to minimize the quantity $\sum w(|F_o| - |F_c|)^2$ with $w = 1/\sigma^2(F)$. Non-hydrogen atoms were refined anisotropically, and hydrogen atoms were included as constant contributions to the structure factors and were not refined. Refinement converged to $R_1 = 0.043$ and $R_2 = 0.056$.

3,4,5-Tridecenoxybenzoic Acid Methyl Ester (General Procedure for 3,4,5-Trialkyloxybenzoic Acid Methyl Esters). 1-Bromodecane (10.00 g, 45.2 mmol) and K_2CO_3 (10.40 g, 75.3 mmol) were added to a 100 mL acetone solution of 2.69 g (14.6 mmol) of 3,4,5-trihydroxybenzoic acid methyl ester containing a catalytic amount of KI, and the mixture was refluxed under N_2 for 3 days. The reaction mixture was then filtered hot, and the acetone was evaporated off leaving a white powder which was recrystallized from THF/acetone to give 7.94 g (90% yield). ^{1}H NMR ($CDCl_3$) 0.87 (t, $OCH_2(CH_2)_8\mathbf{CH_3}$), 1.10−1.82 (m, $OCH_2(\mathbf{CH_2})_8CH_3$), 3.86 (s, $CO_2\mathbf{CH_3}$), 4.00 (t, $O\mathbf{CH_2}(CH_2)_8CH_3$), 7.25 (s, **ArH**). ^{13}C ($CDCl_3$) 166.84, 152.79, 142.33, 124.61, 107.91, 73.41, 69.10, 51.98, 31.92, 30.32, 29.71, 29.37, 29.30, 29.10, 26.06, 22.68, 14.07. IR (thin film) 2935, 1686, 1670, 1582, 1504, 1466, 1428, 1378, 1355, 1331, 1208, 1118, 992 cm^{-1}. MS *m/e* 604 (M^+). Anal. Calcd for $C_{38}H_{68}O_5$: C 75.50, H 11.26. Found C 75.36, H 11.19.

3,4-Didecenoxybenzoic Acid Ethyl Ester (General Procedure for 3,4-Dialkyloxybenzoic Ethyl Esters). 1-Bromodecane (10.81 g, 48.8 mmol) and K_2CO_3 (10.13 g, 73.3 mmol) were added to a 75 mL cyclohexanone solution of 4.24 g (23.3 mmol) of 3,4-dihydroxybenzoic acid ethyl ester with a catalytic amount of potassium iodide, and the solution was refluxed under N_2 for 2 days. The reaction mixture was then filtered hot and cooled and excess methanol was added to precipitate the product which was filtered and recrystallized from THF/acetone to give 9.47 g of white product (88% yield). ^{1}H NMR ($CDCl_3$) 0.86 (t, $OCH_2(CH_2)_8\mathbf{CH_3}$), 1.15−1.93 (m, $OCH_2(\mathbf{CH_2})_8CH_3$ and $CO_2CH_2\mathbf{CH_3}$), 4.01 (t, $O\mathbf{CH_2}(CH_2)_8CH_3$), 4.32 (q, $CO_2\mathbf{CH_2}CH_3$), 6.83 (d, **ArH**), 7.51 (d, **ArH**), 7.63 (dd, **ArH**). ^{13}C ($CDCl_3$) 165.28, 153.07, 148.43, 123.37, 122.70, 114.20, 111.76, 69.12, 68.82, 60.50, 31.77, 30.43, 29.31, 29.21, 29.07, 25.96, 22.61, 14.30, 13.99. IR (thin film) 2975, 1719, 1602, 1515, 1465, 1430, 1478, 1367, 1343, 1288, 1270, 1213, 1173, 1133, 1105, 1030, 764 cm^{-1}. MS *m/e* 462 (M^+). Anal. Calcd for $C_{29}O_4H_{50}$: C 75.32, H 10.91. Found C 75.02, H 10.76.

1,5-Bis(3′,4′,5′-tridecenoxyphenyl)-1,3,5-pentanetrione (General Procedure for 8a). Following the method of Miles et al.[21] 5.00 g (8.4 mmol) of 3,4,5-tridecenoxybenzoic acid methyl ester was added to a 50 mL DME solution containing 0.48 g (4.2 mmol) of acetone and 0.61 g (25.2 mmol) of NaH under N_2 at room temperature. The solution was then refluxed for 1 day, and the resulting pale yellow solution was cooled to room temperature where the excess NaH was quenched with cold water. The solution was then neutralized with a small amount of concentrated HCl, and 50 mL of distilled H_2O was added. The product was extracted with two 50 mL portions of $CHCl_3$ and washed with three 50 mL aliquots of distilled water in a separatory funnel and dried with $MgSO_4$. $CHCl_3$ was evaporated off to leave a yellow solid, which was recrystallized from THF/MeOH to give 4.54 g (90% yield) of product. ^{1}H NMR ($CDCl_3$) 0.88 (t, $OCH_2(CH_2)_8\mathbf{CH_3}$), 1.10−1.87 (m, $OCH_2(\mathbf{CH_2})_8CH_3$), 4.02 (t, $O\mathbf{CH_2}(CH_2)_8CH_3$), [5.89 (s), 6.20 (s)], (OC**CH**CO), [7.01 (s), 7.25 (s)], (**ArH**), [14.82 (s), 16.04 (s)], (**COH**). ^{13}C NMR ($CDCl_3$) 193.56, 192.74, 189.54, 182.77, 173.54, 153.05, 152.93, 152.75, 142.45, 141.55, 130.93, 128.74, 128.43,124.55, 107.90, 107.60, 105.78, 105.06, 96.60, 96.10, 73.32, 69.18, 69.23, 68.95, 31.93, 30.30, 29.67, 29.60, 29.50, 29.37, 26.09, 22.67, 13.98. IR (thin film) 2943, 1677, 1597, 1578, 1497, 1467, 1432, 1378, 1333, 1303, 1243, 1193, 1117, 814, 720 cm^{-1}. MS *m/e* 1203 (M^+). Anal. Calcd for $C_{77}O_9H_{134}$: C 76.87, H 11.14. Found C 76.45, H 11.02.

1,5-Bis(3′,4′-didecenoxyphenyl)-1,3,5-pentanetrione (8b). Yellow powder, yield 93%. ^{1}H NMR ($CDCl_3$) 0.86 (t, $OCH_2(CH_2)_8\mathbf{CH_3}$), 1.10−1.82 (m, $OCH_2(\mathbf{CH_2})_8CH_3$), 4.04 (t, $O\mathbf{CH_2}(CH_2)_8CH_3$), [5.88 (s), 6.21 (s)], (OC**CH**CO), [6.81 (md), 7.50 (md)], (**ArH**), [14.84 (s), 16.10 (s)], (**COH**). ^{13}C ($CDCl_3$) 192.92, 192.45, 188.60, 183.16, 173.36, 154.05, 153.25, 152.31, 148.90, 148.82, 129.17, 126.58, 126.14, 123.94, 121.37, 120.13, 112.58, 112.43, 112.02, 111.85, 111.46, 96.12, 95.45, 69.27, 69.11, 68.97, 31.86, 29.64, 29.31, 29.14, 29.02, 25.93, 24.96, 22.62, 14.04. IR (thin film) 2939, 1686, 1597, 1575, 1500, 1467, 1435, 1381, 1366, 1334, 1245, 1189, 1147, 1121, 1021, 991, 970, 911, 813, 721 cm^{-1}. MS *m/e* 890 (M^+). Anal. Calcd $C_{57}O_7H_{94}$: C 75.07, H 10.80. Found C 75.13, H 10.64.

3,4,5-Tridecenoxybenzoic Acid. To 5.00 g (8.1 mmol) of 3,4,5-tridecenoxybenzoic acid methyl ester in 40 mL of THF was added 0.45 g (16.2 mmol) of a 4 mL aqueous solution of KOH, and the mixture was refluxed under N_2 for 4 h. The reaction mixture was then cooled, and a small amount of concentrated HCl was added to neutralized the mixture. The mixture was evaporated, and the resulting white solid material was washed with distilled H_2O and recrystallized from THF/acetone to give 4.68 g (98% yield) of product. ^{1}H NMR ($CDCl_3$) 0.86 (t, $OCH_2(CH_2)_8\mathbf{CH_3}$), 1.13−1.81 (m, $OCH_2(\mathbf{CH_2})_8CH_3$), 4.00 (t, $O\mathbf{CH_2}(CH_2)CH_3$), 7.30 (s, **ArH**). ^{13}C ($CDCl_3$) 172.25, 152.81, 143.13, 123.70, 108.52, 73.49, 69.12, 31.93, 30.33, 29.71, 29.66, 29.57, 29.39, 29.28, 26.07, 22.70, 14.07. IR (thin film) 2943, 2929, 1683, 1587, 1505, 1466, 1435, 1378, 1335, 1276, 1227, 1150, 1122, 1095, 990, 971, 938, 864, 768, 738, 722 cm^{-1}. MS *m/e* 590 (M^+). Anal. Calcd for $C_{37}O_5H_{66}$: C 75.25, H 11.19. Found C 75.19, H 11.13.

3,4,5-Tridecenoxyacetophenone. Under a nitrogen atmosphere 12.71 mL of a 1.4 M diethyl ether solution of methyl lithium was slowly added to 4.00 g (6.8 mmol) of 3,4,5-tridecenoxybenzoic acid in 30 mL of THF at 0 °C, and the mixture was stirred at this temperature for ½ h. The solution was then warmed to room temperature and stirred for 2 h. This was followed by neutralizing the mixture with a small amount of concentrated HCl. The solvents were evaporated and the remaining solid was washed with distilled H_2O and recrystallized from THF/acetone to give 3.76 g of product (94% yield). ^{1}H NMR ($CDCl_3$) 0.86 (m, $OCH_2(CH_2)_8\mathbf{CH_3}$), 1.23−1.81 (m, $OCH_2(\mathbf{CH_2})_8CH_3$), 2.54 (s, $CO\mathbf{CH_3}$), 4.00 (t, $O\mathbf{CH_2}(CH_2)CH_3$), 7.27 (s, **ArH**). ^{13}C ($CDCl_3$) 196.74, 152.86, 142.87, 132.05, 107.11, 73.41, 69.21, 31.91, 30.33, 29.68, 29.63, 29.54, 29.35, 26.26, 26.06, 22.66, 14.04. IR (thin film) 2934, 1683, 1587, 1505, 1466, 1435, 1378, 1335, 1276, 1227, 1150, 1122, 1095, 990, 971, 938, 864, 768, 738, 722 cm^{-1}. MS 588 (M^+). Anal. Calcd for $C_{38}O_4H_{68}$: C 77.55, H 11.56. Found C 77.31, H 11.19.

1-(3′,4′,5′-Tridecenoxyphenyl)-1,3-butanedione. Under an atmosphere of N_2 at room temperature 3.00 g (5.1 mmol) of 3,4,5-tridecenoxyacetophenone was added to 50 mL of ethyl acetate (excess) containing 1.04 g (15.3 mmol) of NaOEt. The same reaction conditions and workup procedure reported for **8a** were followed to give 2.86 g (89% yield) of the product as a yellow powder. ^{1}H NMR ($CDCl_3$) 0.86 (t, $OCH_2(CH_2)_8\mathbf{CH_3}$), 1.23−1.80 (m, $OCH_2(\mathbf{CH_2})_8CH_3$), 2.16 (s, $OC\mathbf{CH_3}$), 4.00 (t, $O\mathbf{CH_2}(CH_2)_8CH_3$), 6.07 (s, OC**CH**CO), 7.07 (s, **ArH**), 16.24 (s, **COH**). ^{13}C NMR ($CDCl_3$) 193.06, 192.48, 191.36, 189.38, 184.39, 182.65, 173.42, 152.99, 152.87, 152.72, 141.49, 130.90, 129.76, 128.69, 128.35, 107.50, 105.68, 104.94, 96.50, 96.03,

73.41, 69.10, 31.89, 29.70, 29.64, 29.36, 28.46, 26.06, 25.04, 22.64, 14.01. IR (thin film) 2933, 1676, 1657, 1577, 1496, 1463, 1432, 1378, 1336, 1240, 1191, 1154, 1119, 993, 954, 910, 859, 841, 815, 776, 723, 706 cm^{-1}. MS *m/e* 630 (M^+). Anal. Calcd for $C_{40}O_5H_{70}$: C 76.19, H 11.11. Found C 75.89, H 11.42.

1-(3′,4′,5′-Tridecenoxyphenyl)-5-(3″,4″-didecenoxyphenyl)-1,3,5-pentanetrione (9). 3,4-Didecenoxybenzoic acid ethyl ester (2.95 g, 4.8 mmol) was added to a DME solution containing 3.00 g (4.8 mmol) of 1-(3′,4′,5′-tridecenoxyphenyl)-1,3-butanedione and 0.11 g (13.6 mmol) of NaH under N_2 at room temperature. The same reaction conditions and workup procedure reported for **8a** were followed to give 4.26 g (85%) of the product as a yellow powder. ^1H NMR ($CDCl_3$) 0.88 (t, $OCH_2(CH_2)_8\mathbf{CH_3}$), 1.10−1.91 (m, $OCH_2\mathbf{(CH_2)_8}CH_3$), 4.00 (t, $O\mathbf{CH_2}(CH_2)_8CH_3$), [6.10 (s), 6.18 (s), 6.22 (s), 6.26 (s)], (OC**CH**CO), [6.81 (md), 7.04 (s), 7.30 (s), 7.51 (md)], (**ArH**), [14.80 (s), 14.90 (s), 16.02 (s), 16.21 (s)], (**COH**). ^{13}C NMR ($CDCl_3$) 193.00, 192.74, 192.30, 189.54, 188.39, 183.16, 182.79, 173.74, 173.16, 154.07, 153.31, 153.04, 152.92, 152.80, 152.43, 148.93, 148.81, 143.34, 141.43, 130.96, 129.14, 128.84, 128.55, 126.02, 123.96, 121.38, 120.20, 112.58, 112.40, 112.00, 111.84, 111.44, 107.60, 105.77, 105.00, 96.64, 96.14, 96.09, 95.46, 73.51, 69.19, 68.97, 31.87, 30.30, 29.90, 29.68, 29.54, 29.31, 29.22, 29.16, 29.07, 28.95, 26.09, 25.96, 22.64, 14.06. IR (thin film) 2933, 1677, 1592, 1569, 1516, 1500, 1466, 1378, 1337, 1271, 1196, 1151, 1132, 1121, 1075, 1048, 1023, 989, 936, 893, 848, 810, 796, 776, 723 cm^{-1}. MS *m/e* 1047 (M^+). Anal. Calcd for $C_{67}O_8H_{114}$: C 76.79, H 10.89. Found C 76.32, H 10.93.

1,7-Bis(3′,4′,5′-tridecenoxyphenyl)-1,3,5,7-heptanetetraone (General Procedure for 10). 2,4-Pentanedione (0.29 g, 2.9 mmol) was added to a 35 mL DME solution containing 3.50 g (5.8 mmol) of 3,4,5-tridecenoxybenzoic acid methyl ester and 0.42 g (17.4 mmol) of NaH under N_2 at room temperature. The same reaction conditions and workup procedures reported for **8a** were followed to give 3.12 g (85%) of the product as a yellow powder. ^1H NMR ($CDCl_3$) 0.86 (t, $OCH_2(CH_2)_8\mathbf{CH_3}$), 1.12−1.94 (m, $OCH_2\mathbf{(CH_2)_8}CH_3$), 3.51 (s, $OC\mathbf{CH_2}CO$), 3.99 (t, $O\mathbf{CH_2}(CH_2)_8CH_3$), 6.23 (s, OC**CH**CO), 7.07 (s, **ArH**), 16.04 (s, **COH**). ^{13}C NMR ($CDCl_3$) 193.09, 192.62, 188.77, 183.60, 171.51, 153.05, 142.99, 142.50, 130.95, 128.87, 123.69, 108.42, 107.60, 105.84, 96.60, 96.12, 73.52, 69.24, 69.07, 69.06, 31.91, 30.30, 29.70, 29.55, 29.37, 26.06, 22.66, 14.06. IR (thin film) 2936, 1684, 1586, 1500, 1467, 1461, 1435, 1378, 1335, 1278, 1231, 1120, 864, 722 cm^{-1}. MS *m/e* 1245 (M^+). Anal. Calcd for $C_{79}O_{10}H_{136}$: C 76.14, H 11.01. Found C 76.12, H 11.07.

1-(3′,4′,5′-Tridecenoxyphenyl)-1,3,5-hexanetrione (General Procedure for 11a). 3,4,5-Tridecenoxybenzoic acid methyl ester (3.00 g, 5.0 mmol) was added to a 30 mL DME solution containing 0.50 g (5.0 mmol) of 2,4-pentanedione and 0.12 g (15.0 mmol) of NaH under N_2 at room temperature. The same reaction conditions and workup procedures reported for **8a** were followed to give a yellow powder, 3.03 g (90% yield). ^1H NMR ($CDCl_3$) 0.86 (t, $OCH_2(CH_2)_8\mathbf{CH_3}$), 1.12−1.82 (m, $OCH_2\mathbf{(CH_2)_8}CH_3$), [1.94 (s), 1.97 (s), 2.24 (s), 2.28 (s)], (OC$\mathbf{CH_3}$), [3.45(s), 3.83 (s)], (OC$\mathbf{CH_2}$CO), 3.99 (t, $O\mathbf{CH_2}(CH_2)_8CH_3$), [5.28 (s), 5.60 (s), 5.70 (s), 6.11 (s)], (OC**CH**CO), [7.05 (s), 7.12 (s), 7.19 (s), 7.29 (s)], (**ArH**), [14.11 (s), 14.53 (s), 14.83 (s), 15.30 (s), 16.04 (s)], (**COH**). ^{13}C ($CDCl_3$) 193.45, 192.50, 186.92, 184.39, 178.07, 173.90, 153.02, 152.93, 143.40, 142.57, 141.50, 130.93, 128.99, 128.37, 107.49, 105.85, 105.00, 100.58, 99.40, 96.85, 95.20, 73.50, 69.23, 69.18, 54.36, 31.86, 30.28, 30.19, 29.54, 29.31, 29.23, 26.03, 23.92, 22.63, 21.78, 14.04. IR (thin film) 2919, 1720, 1686, 1597, 1575, 1503, 1467, 1435, 1381, 1366, 1334, 1245, 1189, 1147, 1121, 1021, 991, 970, 911, 813, 721 cm^{-1}. MS *m/e* 673 (M^+). Anal. Calcd $C_{42}O_6H_{72}$: C 74.89, H 10.70. Found C 75.03, H 10.64.

1-(3′,4′-Dihexadecenoxyphenyl)-1,3,5-hexanetrione (11b). Yellow powder, yield 89%. ^1H NMR ($CDCl_3$) 0.86 (t, $OCH_2(CH_2)_{14}\mathbf{CH_3}$), 1.10−1.85 (m, $OCH_2\mathbf{(CH_2)_{14}}CH_3$), [1.99 (s), 2.01 (s), 2.24 (s), 2.28 (s)], (OC$\mathbf{CH_3}$), [3.49(s), 3.89, (s)], (OC$\mathbf{CH_2}$CO), 3.99 (t, $O\mathbf{CH_2}(CH_2)_{14}CH_3$), [5.30 (s), 5.61 (s), 5.71 (s), 6.14 (s)], (OC**CH**CO), [6.81 (md), 7.43 (md)], **ArH**), [14.02 (s), 14.93 (s), 15.20 (s), 16.13 (s)], (**COH**). ^{13}C ($CDCl_3$) 195.60, 193.25, 192.56, 187.23, 185.46, 180.32, 177.54, 167.32, 153.45, 149.22, 147.89, 143.45, 142.63, 137.24, 130.95, 127.83, 126.58, 123.53, 121.51, 118.34, 112.40, 111.82, 111.40, 102.35, 99.83, 96.50, 94.55, 69.30, 70.00, 69.83, 54.27, 31.90, 29.60, 29.34, 29.16, 29.00, 25.95, 22.68, 23.92, 21.78, 14.10. IR (thin film) 2917, 1720, 1686, 1597, 1575, 1500, 1467, 1435, 1381, 1366, 1334, 1245, 1189, 1147, 1121, 1021, 991, 970, 911, 813, 721 cm^{-1}. MS *m/e* 684 (M^+). Anal. Calcd $C_{44}O_5H_{76}$: C 77.19, H 11.11. Found C 77.13, H 10.94.

1,1,1-Trifluoro-5-(3′,4′,5′-tridecenoxyphenyl)-1,3,5-hexanetrione (General Procedure for 12). 3,4,5-Tridecenoxybenzoic acid methyl ester (1.93 g, 3.2 mmol) was added to a 30 mL DME solution of 0.49 g (3.2 mmol) of 1,1,1-trifluoro-2,4-pentanedione and 77.5 mg (9.6 mmol) of NaH under N_2 at room temperature. The reaction conditions and workup procedures were followed as for **8a** to give a yellow powder, 2.11 g (82% yield). ^1H NMR ($CDCl_3$) 0.86 (t, $OCH_2(CH_2)_8\mathbf{CH_3}$), 1.14−1.91 (m, $OCH_2\mathbf{(CH_2)_8}CH_3$), [3.50 (s), 3.82 (s)], (OC$\mathbf{CH_2}$-CO), 3.99 (t, $O\mathbf{CH_2}(CH_2)_8CH_3$), [5.76 (s), 5.87 (s), 6.00 (s), 6.13 (s)], (OC**CH**CO), [6.87 (s), 6.90 (s), 7.07 (s), 7.14 (s)], (**ArH**), [14.19 (s), 14.93 (s), 15.32 (s), 16.14 (s)], (**COH**). ^{13}C ($CDCl_3$) 193.38, 178.19, 153.54, 153.12, 148.90, 127.11, 124.72, 123.35, 121.16, 112.23, 111.79, 111.61, 105.52, 99.41, 96.20, 95.55, 73.59, 69.32, 69.00, 60.61, 31.84, 30.24, 29.62, 29.29, 29.10, 28.95, 25.91, 22.60, 14.02. IR (thin film) 2932, 1720, 1665, 1630, 1592, 1572, 1515, 1462, 1445, 1378, 1335, 1300, 1277, 1252, 1236, 1209, 1196, 1173, 1144, 1133, 1061, 1018, 722 cm^{-1}. MS *m/e* 726 (M^+). Anal. Calcd $C_{42}O_6H_{69}F_3$: C 69.49, H 9.50, F 7.85. Found C 69.84, H 9.67, F 7.69.

1-(3′,4′,5′-Tridodecenoxyphenyl)-1,3,5,7-octanetetraone (13a). 1,3,5-Heptanetrione (1.01 g, 7.1 mmol) was added to a 25 mL DME solution containing 4.88 g (7.1 mmol) of 3,4,5-tridodecenoxybenzoic acid methyl ester and 0.51 g (21.3 mmol) of NaH under N_2 at room temperature. The reaction conditions and workup procedures were followed as for **8a** to give a yellow powder, 4.10 g (73% yield). ^1H NMR ($CDCl_3$) 0.86 (t, $OCH_2(CH_2)_{10}\mathbf{CH_3}$), 1.13−1.86 (m, $OCH_2\mathbf{(CH_2)_{10}}CH_3$), [1.93 (s), 1.96 (s), 2.07 (s), 2.15 (s), 2.28 (s), 2.54 (s)], (OC$\mathbf{CH_3}$), [3.33 (s), 3.42 (s), 3.85 (s)], (OC$\mathbf{CH_2}$CO), 3.99 (t, $O\mathbf{CH_2}(CH_2)_{10}CH_3$), [5.22 (s), 5.34 (s), 5.55 (s), 5.76 (s), 6.12 (s), 6.18 (s)], (OC**CH**CO), [6.83 (s), 6.95 (s), 7.07 (s), 7.17 (s), 7.21 (s), 7.27 (s)], (**ArH**), [13.93 (s), 14.06 (s), 14.46 (s), 14.88 (s), 15.22 (s), 16.03 (s)], (**COH**). ^{13}C NMR ($CDCl_3$) 194.25, 192.62, 190.54, 189.67, 182.77, 178.54, 173.54, 168.92, 153.23, 152.65, 142.89, 142.17, 141.55, 130.93, 128.74, 128.43, 123.66, 107.83, 107.45, 105.61, 105.00, 99.73, 96.72, 96.07, 73.49, 69.43, 69.32, 69.02, 31.91, 30.27, 29.63, 29.55, 29.29, 25.95, 22.59, 14.00. IR (thin film) 2923, 1726, 1683, 1588, 1505, 1467, 1461, 1456, 1445, 1436, 1379, 1335, 1277, 1229, 1123, 990, 970, 864, 768, 721 cm^{-1}. MS *m/e* 792 (M^+). Anal. Calcd for $C_{50}O_7H_{86}$: C 75.75, H 10.94. Found C 75.45, H 11.02.

1-(3′,4′-Didodecenoxyphenyl)-1,3,5,7-octanetetraone (13b). Yellow powder, 62%. ^1H NMR ($CDCl_3$) 0.86 (t, $OCH_2(CH_2)_{10}\mathbf{CH_3}$), 1.13−1.86 (m, $OCH_2\mathbf{(CH_2)_{10}}CH_3$), [1.96 (s), 2.04 (s), 2.14 (s), 2.22 (s), 2.24 (s), 2.53 (s)], (OC$\mathbf{CH_3}$), [3.29 (s), 3.36 (s), 3.78 (s)], (OC$\mathbf{CH_2}$CO), 3.99 (t, $O\mathbf{CH_2}(CH_2)_{10}CH_3$), [5.36 (s), 5.65 (s), 5.73 (s), 6.09 (s), 6.17 (s), 6.21 (s)], (OC**CH**CO), [6.82 (md), 7.42 (md)], (**ArH**), [14.08 (s), 14.16 (s), 14.46 (s), 14.91 (s), 15.21 (s), 16.09 (s)], (**COH**). ^{13}C NMR ($CDCl_3$) 195.00, 192.62, 190.54, 189.67, 184.77, 178.54, 173.54, 168.92, 153.87, 148.48, 142.89, 142.17, 141.55, 130.93, 124.34, 121.50, 121.28, 114.47, 114.23, 111.98, 111.79, 105.61, 105.00, 99.73, 96.72, 96.07, 73.49, 69.43, 69.32, 69.02, 31.89, 30.27, 29.63, 29.55, 29.29, 25.95, 22.59, 14.00. IR (thin film) 2935, 1721, 1690, 1588, 1505, 1465, 1467, 1449, 1441, 1430, 1373, 1332, 1272, 1229, 1123, 991, 970, 864, 768, 721 cm^{-1}. MS *m/e* 614 (M^+). Anal. Calcd for $C_{38}O_6H_{62}$: C 74.27, H 10.17. Found C 74.86, H 9.83.

(General Procedure for 14a). This Schiff-base derivative was prepared by adding a 2 mL methanolic solution containing 68.4 mg (1.1 mmol, 7.6×10^{-2} mL) of ethylenediamine dropwise to a solution of 1.53 g of **11a** (2.3 mmol, where n = 10) in 20 mL of $CHCl_3$ and allowing the reaction mixture to stir for 12 h at room temperature under N_2. The solvent was evaporated and the resulting yellow solid was recrystallized from THF/ethyl acetate to give 1.35 g (91% yield). ^1H NMR ($CDCl_3$) 0.85 (t, $OCH_2(CH_2)_8\mathbf{CH_3}$), 1.02−1.86 (m, $OCH_2\mathbf{(CH_2)_8}$-CH_3), [1.81 (s), 1.86 (s), 1.92 (s), 1.98 (s)], (NC$\mathbf{CH_3}$), 3.42 (m, $\mathbf{N(CH_2)_2}N$), [3.83 (s), 3.85 (s)], (OC$\mathbf{CH_2}$CO), 4.00 (t, $O\mathbf{CH_2}(CH_2)_8$-CH_3), [4.76 (s), 4.80 (s), 5.05 (s), 5.07 (s), 5.67 (s), 5.68 (s)], (OC**CH**CO), [6.95 (s), 7.25 (s)], (**ArH**), [10.24 (s), 10.26 (s),

10.83 (s), 10.91 (s), 15.83 (s), 15.90 (s)], (**COH**). ^{13}C ($CDCl_3$) 194.15, 190.06, 189.34, 189.22, 170.63, 164.48, 164.31, 162.46, 152.83, 152.69, 142.75, 140.33, 131.49, 129.74, 107.48, 104.33, 96.21, 95.60, 73.32, 68.98, 53.65, 53.49, 43.64, 43.38, 31.78, 30.21, 29.51, 29.26, 26.00, 22.54, 19.02, 18.57, 18.45, 13.95. IR (thin film) 3194, 2923, 1673, 1578, 1505, 1467, 1439, 1406, 1378, 1338, 1281, 1239, 1165, 1122, 1029, 800, 720 cm^{-1}. MS *m/e* 1369 (M^+). Anal. Calcd for $C_{86}O_{10}H_{148}N_2$: C 75.44, H 10.82, N 2.05. Found C 75.17, H 10.65, N 1.94.

14b. Yield 93%, yellow powder. ^{1}H NMR ($CDCl_3$) 0.85 (t, $OCH_2(CH_2)_{14}\mathbf{CH_3}$), 1.10–1.90 (m, $OCH_2\mathbf{(CH_2)_{14}}CH_3$), [1.89 (s), 1.91 (s), 1.95 (s), 1.98 (s)], (NC**CH$_3$**), 3.43 (m, N**(CH$_2$)$_2$**N), [3.84 (s), 3.86 (s)], (OC**CH$_2$**CO), 4.02 (t, O**CH$_2$**$(CH_2)_{14}CH_3$), [4.78 (s), 4.80 (s), 5.02 (s), 5.08 (s), 5.67 (s), 4.68 (s)], (OC**CH**CO), [6.82 (md), 7.62 (md)], (**ArH**), [10.18 (s), 10.24 (s), 10.83 (s), 10.95 (s), 15.93 (s), 15.97 (s)], (**COH**). ^{13}C ($CDCl_3$) 193.68, 191.42, 190.65, 190.34, 178.53, 172.20, 165.10, 163.45, 163.94, 159.78, 152.07, 149.57, 149.24, 148.87, 148.75, 129.67, 124.02, 121.40, 120.67, 119.61, 113.97, 119.38, 114.03, 113.90, 113.29, 113.07, 112.91, 111.58, 111.48, 111.02, 109.40, 103.56, 96.27, 95.55, 69.50, 69.30, 69.13, 53.23, 52.85, 44.00, 42.95, 39.69, 31.89, 30.30, 30.06, 29.63, 29.35, 26.07, 22.65, 19.10, 18.73, 14.04. IR (thin film) 3200, 2923, 1673, 1578, 1502, 1463, 1443, 1408, 1380, 1338, 1284, 1239, 1168, 1122, 1029, 802, 722 cm^{-1}. MS *m/e* 1392 (M^+). Anal. Calcd $C_{90}O_8H_{156}N_2$: C 77.59, H 11.21, N 2.01. Found C 77.45, H 11.19, N 1.85.

General Procedure for 14c. Prepared using an analogous procedure as in the preparation of **14a** (n = 10). Yield 88%, yellow powder. ^{1}H NMR ($CDCl_3$) 0.82 (t, $OCH_2(CH_2)_8\mathbf{CH_3}$), 1.08–1.86 (m, $OCH_2\mathbf{(CH_2)_8}CH_3$, $NCH_2\mathbf{CH_2}CH_2N$), [1.88 (s), 1.92 (s), 1.99 (s), (NC**CH$_3$**), 3.33 (m, N**CH$_2$**CH_2**CH$_2$**N), [3.83 (s), 3.84 (s)], (OC**CH$_2$**CO), 4.00 (t, O**CH$_2$**$(CH_2)_8CH_3$), [4.76 (s), 4.80 (s), 5.04 (s), 5.08 (s), 5.66 (s), 5.68 (s)], (OC**CH**CO), [6.95 (s), 7.25 (s)], (**ArH**), [9.24 (s), 9.26 (s), 10.22 (s), 10.24 (s), 10.84 (s), 10.89 (s)], (**COH**). ^{13}C ($CDCl_3$) 193.89, 190.12, 189.53, 189.22, 170.80, 164.49, 164.39, 162.31, 153.54, 151.28, 148.71, 129.70, 127.45, 124.00, 119.20, 112.54, 111.40, 111.03, 95.61, 95.44, 69.16, 68.97, 68.85, 53.39, 43.62, 43.39, 31.86, 29.54, 29.10, 28.98, 25.97, 22.63, 18.98, 18.63, 18.51, 14.04. IR (thin film) 3194, 2915, 1673, 1578, 1505, 1467, 1439, 1406, 1378, 1338, 1281, 1239, 1165, 1122, 1029, 800, 720 cm^{-1}. MS *m/e* 1383 (M^+). Anal. Calcd for $C_{87}O_{10}H_{150}N_2$: C 75.49, H 10.93, N 2.02. Found C 75.17, H 10.65, N 1.94.

14d. Prepared using the analogous procedure as **14a** (n = 10). Yield 86%, yellow powder. ^{1}H NMR ($CDCl_3$) 0.86 (t, $OCH_2(CH_2)_{10}\mathbf{CH_3}$), 1.10–1.92 (m, $OCH_2\mathbf{(CH_2)_{10}}CH_3$, NHC-**(CH$_2$)$_4$**CHN(cyclohexyl)), [1.75 (s), 1.84 (s), 1.91 (s)], (NC**CH$_3$**), 3.61 (m, N**HC**$(CH_2)_4$**CH**N(cyclohexyl)), [3.82 (s), 3.91 (s)], (OC**CH$_2$**CO), 3.96 (t, O**CH$_2$**$(CH_2)_{10}CH_3$), [4.74 (s), 4.79 (s), 4.93 (s), 4.96 (s), 5.61 (s), 5.64 (s)], (OC**CH**CO), [6.90 (s), 7.25 (s)], (**ArH**), [10.42 (s), 10.45 (s), 11.02 (s), 11.08 (s), 15.95 (s), 15.98 (s)], (**COH**). ^{13}C ($CDCl_3$) 194.21, 189.89, 188.76, 170.72, 163.80, 161.4, 152.87, 152.74, 142.32, 140.50, 131.72, 130.45, 128.00, 107.57, 104.45, 95.83, 95.62, 73.41, 69.08, 53.49, 53.42, 43.64, 43.64, 43.38, 31.86, 30.28, 29.65, 29.31, 26.06, 22.62, 18.91, 18.83, 14.03. IR (thin film) 3197, 2929, 1673, 1572, 1500, 1466, 1436, 1378, 1334, 1305, 1269, 1239, 1164, 1117, 979, 854, 722 cm^{-1}. MS *m/e* 1591 (M^+). Anal. Calcd for $C_{102}O_{10}H_{178}N_2$: C 76.93, H 11.28, N 1.76. Found C 76.84, H 11.02, N 1.56.

14e. Prepared using the analogous procedure as in the preparation of **14a** (n = 10). Yield 81%, yellow powder. ^{1}H NMR ($CDCl_3$) 0.86 (t, $OCH_2(CH_2)_{10}\mathbf{CH_3}$), 1.14–1.90 (m, $OCH_2\mathbf{(CH_2)_{10}}CH_3$, $NH_2CC\mathbf{(CH_3)_2}CH_2N$), [1.77 (s), 1.83 (s), 1.91 (s)], (NC**CH$_3$**), 3.46 (m, N**H$_2$**C$C(CH_3)_2$**CH$_2$**N), [3.89 (s), 3.91 (s)], (OC**CH$_2$**CO), 4.00 (t, O**CH$_2$**$(CH_2)_{10}CH_3$), [4.73 (s), 4.75 (s), 4.97 (s), 4.99 (s), 5.56 (s), 5.58 (s)], (OC**CH**CO), [6.89 (s), 7.25 (s)], (**ArH**), [9.34 (s), 9.36 (s), 10.21 (s), 10.23 (s), 10.87 (s), 10.90 (s)], (**COH**). ^{13}C ($CDCl_3$) 194.10, 190.17, 189.56, 189.23, 170.80, 164.53, 164.42, 162.33, 153.57, 151.32, 148.76, 129.75, 127.45, 124.11, 119.23, 112.50, 111.47, 111.13, 95.66, 95.47, 69.23, 69.03, 68.85, 53.41, 43.65, 31.78, 29.54, 29.30, 29.07, 28.85, 26.03, 22.63, 19.03, 18.66, 18.53, 15.07, 14.00. IR (thin film) 3198, 2943, 1673, 1578, 1505, 1467, 1439, 1406, 1378, 1338, 1281, 1239, 1165, 1122, 1029, 800, 720 cm^{-1}. MS *m/e* 1579 (M^+). Anal. Calcd for $C_{101}O_{10}H_{178}N_2$: C 76.76, H 11.27, N 1.77. Found C 76.17, H 10.65, N 1.94.

15. Yellow powder, yield 79%. ^{1}H NMR ($CDCL_3$) 0.86 (t, $OCH_2(CH_2)_{10}\mathbf{CH_3}$), 1.10–1.86 (m, $OCH_2\mathbf{(CH_2)_{10}}CH_3$), [1.89 (s), 2.25 (s)], (NC**CH$_3$**), 3.40 (m, N**(CH$_2$)$_2$**N), [3.82 (s), 3.85 (s)], (OC**CH$_2$**CO), 4.00 (t, O**CH$_2$**$(CH_2)_{10}CH_3$), [4.94 (s), 5.01 (s), 5.63 (s), 5.67 (s)], (OC**CH**CO), [6.85 (s), 7.29 (s)], (**ArH**), [10.91 (s), 10.93 (s), 11.57 (s), 11.60 (s)], (**COH**). ^{13}C ($CDCl_3$) 193.23, 189.92, 187.30, 170.25, 166.53, 165.25, 162.46, 152.28, 150.37, 142.54, 141.65, 131.95, 129.25, 128.06, 107.53, 105.21, 100.35, 96.34, 95.21, 69.15, 68.90, 60.56, 41.44, 31.83, 30.21, 29.55, 29.50, 29.30, 29.10, 25.95, 22.94, 18.93, 18.59, 18.48, 14.00. IR (thin film) 3194, 2943, 1678, 1582, 1503, 1462, 1438, 1423, 1401, 1383, 1338, 1281, 1240, 1165, 1121, 1031, 798, 723 cm^{-1}. MS *m/e* 1621 (M^+). Anal. Calcd for $C_{102}O_{12}H_{176}N_2$: C 75.51, H 10.94, N 1.73. Found C 75.23, H 10.73, N 1.52.

General Method for the Synthesis of Binuclear Copper Complexes: For 1a, 1b, 1c, 2a, 2b, 2c, 4, and 5. The yellow ketonate ligands (0.0010 mol) were dissolved in a minimum volume of hot chloroform (5 mL) to which was added 20 mL a hot green methanolic solution of cupric acetate monohydrate (0.0011). For **3a, 3b, 3c, 3d, 3e, and 6,** 0.0022 mol of cupric acetate monohydrate was used. The solutions immediately turned green and were refluxed for 3 h and cooled, and excess MeOH was added to precipitate green or brown products. The products are filtered, washed with methanol, and recrystallized from THF/acetone. Only representative compounds of the homologous series are given here.

1a, n = 10. Yield 93%. IR (thin film) 2935, 1588, 1545, 1531, 1491, 1455, 1396, 1379, 1342, 1321, 1270, 1182, 1125, 989, 880, 872, 804, 725, 685 cm^{-1}. MS 2528 (M^+). Anal. Calcd for $C_{154}O_{18}H_{264}Cu_2$: C 73.85, H 10.51, Cu 5.02. Found C 74.27, H 10.94, Cu 4.73.

1b, n = 10. Yield 92%. IR (thin film) 2943, 1594, 1553, 1537, 1515, 1504, 1448, 1399, 1387, 1336, 1296, 1279, 1255, 1184, 1153, 1130, 1120, 1093, 1070, 1047, 1023, 987, 934, 883, 862, 825, 794, 767, 739, 722, 698, 673, 662 cm^{-1}. MS 2216 (M^+). Anal. Calcd for $C_{134}O_{16}H_{224}Cu_2$: C 72.53, H 10.18, Cu 5.73. Found C 72.57, H 10.00, Cu 5.71.

1c, n = 10. Yield 89%. IR (thin film) 2945, 1594, 1562, 1535, 1508, 1465, 1401, 1395, 1334, 1305, 1270, 1245, 1196, 1187, 1155, 1130, 1120, 1104, 1090, 1070, 1047, 1023, 994, 889, 797, 767, 729, 713, 698, 676 cm^{-1}. MS 1903 (M^+). Anal. Calcd for $C_{114}O_{14}H_{184}Cu_2$: C 71.90, H 9.74, Cu 6.67. Found C 72.13, H 9.88, Cu 6.43.

4, n = 10. Yield 73%. IR (thin film) 3468, 2946, 1580, 1534, 1495, 1473, 1450, 1411, 1389, 1331, 1240, 1228, 1185, 1160, 1132, 1119, 990, 818, 802, 717 cm^{-1}. MS 2612 (M^+). Anal. Calcd for $C_{158}O_{20}H_{268}Cu_2$: C 71.90, H 9.74, Cu 6.67. Found C 71.23, H 9.55, Cu 6.64.

2a, n = 10. Yield 89%. IR (thin film) 2923, 1590, 1538, 1503, 1453, 1404, 1382, 1335, 1269, 1226, 1179, 1124, 1028, 992, 857, 794, 723 cm^{-1}. MS 1467 (M^+). Anal. Calcd for $C_{84}O_{12}H_{140}Cu_2$: C 68.66, H 9.61, Cu 8.66. Found C 68.57, H 9.77, Cu 8.53.

2b, n = 10. Yield 95%. IR (thin film) 2933, 1590, 1581, 1538, 1489, 1460, 1446, 1382, 1333, 1290, 1227, 1191, 1127, 989, 904, 861, 811, 769, 740, 719, 684, 670 cm^{-1}. MS 1574 (M^+). Anal. Calcd for $C_{84}O_{12}H_{134}Cu_2F_6$: C 63.99, H 8.51, Cu 8.07, F 3.62. Found C 63.85, H 8.23, Cu 8.03, F 3.58.

2c, n = 16. Yield 87%. IR (thin film) 2945, 1590, 1581, 1538, 1489, 1460, 1446, 1382, 1333, 1290, 1227, 1191, 1127, 989, 904, 861, 811, 769, 740, 719, 684, 670 cm^{-1}. MS 1491 (M^+). Anal. Calcd for $C_{88}O_{10}H_{148}Cu_2$: C 70.78, H 10.00, Cu 8.52. Found C 70.32, H 9.39, Cu 8.19.

5a, n = 12. Yield 75%. IR (thin film) 3496, 2949, 1588, 1533, 1499, 1456, 1451, 1389, 1379, 1339, 1323, 1263, 1248, 1228, 1177, 1148, 1123, 986, 858, 793, 722 cm^{-1}. MS 1719 (M^+). Anal. Calcd for $C_{100}O_{14}H_{168}Cu_2$: C 69.73, H 9.76, Cu 7.38. Found C 69.54, H 9.75, Cu 7.15.

5b, n = 12. Yield 67%. IR (thin film) 3445, 2944, 1589, 1533, 1502, 1456, 1448, 1389, 1384, 1345, 1323, 1263, 1248, 1228, 1177, 1151, 1129, 1018, 986, 858, 790, 726 cm^{-1}. MS 1350 (M^+). Anal. Calcd for $C_{76}O_{12}H_{120}Cu_2$: C 67.55, H 8.96, Cu 9.33. Found C 67.47, H 8.22, Cu 8.85.

3a, n = 10. Yield 95%. IR (thin film) 2943, 1569, 1528, 1503, 1475, 1436, 1382, 1335, 1247, 1225, 1178, 1114, 1038, 991, 854, 783, 718, cm^{-1}. MS 1491 (M^+). Anal. Calcd for C_{86}-

$O_{10}H_{144}Cu_2N_2$: C 69.18, H 9.72, Cu 8.51, N 1.88. Found C 69.52, H 10.14, N 1.88, Cu 8.34.

3b, n = 10. Yield 88%. IR (thin film) 2943, 1567, 1528, 1503, 1471, 1436, 1379, 1330, 1276, 1219, 1177, 1113, 1038, 989, 850, 800, 786, 723 cm^{-1}. MS 1505 (M^+). Anal. Calcd for $C_{87}O_{10}H_{146}Cu_2N_2$: C 69.33, H 9.76, Cu 8.43, N 1.86. Found C 69.38, H 9.82, Cu 8.44, N 1.82.

3c, n = 16. Yield 93%. IR (thin film) 2943, 1599, 1533, 1510, 1466, 1436, 1378, 1336, 1269, 1194, 1141, 1069, 1023, 977, 874, 800, 778, 722 cm^{-1}. MS 1515 (M^+). Anal. Calcd for $C_{90}O_8H_{152}N_2Cu_2$: C 71.29, H 10.03, N 1.85, Cu 8.39. Found C 70.95, H 9.83, N 1.76, Cu 8.27.

3d, n = 12. Yield 86%. IR (thin film) 2945, 1559, 1489, 1473, 1430, 1385, 1365, 1333, 1285, 1228, 1180, 1147, 1117, 991, 864, 763, 722 cm^{-1}. MS 1713 (M^+). Anal. Calcd for $C_{102}O_{10}H_{174}Cu_2N_2$: C 71.41, H 10.23, N 1.63, Cu 7.41. Found C 71.66, H 10.21, N 1.53, Cu 7.22.

3e, n = 12. Yield 88%. IR (thin film) 2929, 1565, 1521, 1507, 1467, 1433, 1379, 1333, 1279, 1214, 1172, 1111, 1035, 991, 852, 823, 786, 727 cm^{-1}. MS 1701 (M^+). Anal. Calcd for $C_{101}O_{10}H_{174}Cu_2N_2$: C 71.21, H 10.30, Cu 7.47, N 1.65. Found C 71.38, H 9.82, Cu 7.44, N 1.52.

6, n = 12. Yield 83%. IR (thin film) 3538, 2934, 1586, 1536, 1503, 1475, 1462, 1391, 1376, 1343, 1325, 1264, 1248, 1230, 1180, 1148, 1123, 986, 860, 793, 724 cm^{-1}. MS 1743 (M^+). Anal. Calcd for $C_{102}O_{12}H_{172}Cu_2N_2$: C 70.22, H 9.87, Cu 7.29, N 1.61. Found C 70.12, H 9.34, Cu 7.16, N 1.53.

General Procedure for 16, n = 14. To 0.30 g (0.2 mmol) of **14a** in 5 mL of a THF solution was slowly added 20 mL of a hot 49.7 mg (0.2 mmol) methanolic solution of nickel acetate tetrahydrate. The solution immediately turned brown and was refluxed for 0.5 h. The solvent was evaporated and the resulting brown solid was recrystallized from THF/acetone to give 0.29 g (81% yield). ^1H NMR ($CDCl_3$) 0.86 (t, $OCH_2(CH_2)_{12}\mathbf{CH_3}$), 1.12–1.89 (m, $OCH_2(\mathbf{CH_2})_{12}CH_3$), [1.76 (s), 1.82 (s), 1.88 (s)], ($NC\mathbf{CH_3}$), [2.95 (s), 2.99 (s)], ($OC\mathbf{CH_2}CO$), [3.70 (s), 3.72 (s)], ($N(\mathbf{CH_2})_2N$), 3.98 (m, $O\mathbf{CH_2}(CH_2)_{12}CH_3$), [4.83 (s), 4.90 (s), 4.94 (s), 5.34 (s)], ($OC\mathbf{CH}CO$), [6.82 (s), 7.25 (s), 7.31 (s)], (**ArH**), 12.62 (s, **COH**). ^{13}C ($CDCl_3$) 196.00, 194.40, 187.54, 171.98, 171.49, 170.98, 165.22, 164.37, 152.83, 152.74, 142.71, 140.01, 131.27, 131.00, 107.53, 107.14, 103.99, 100.00, 98.67, 94.61, 73.38, 68.14, 53.70, 31.86, 30.32, 29.66, 29.31, 26.12, 26.02, 22.62, 21.39, 21.18, 14.02. IR (thin film) 3276, 2914, 1671, 1619, 1582, 1505, 1493, 1466, 1478, 1336, 1230, 1180, 1117, 1050, 1019, 997, 819, 722 cm^{-1}. MS *m/e* 1762 (M^+). Anal. Calcd for $C_{110}O_{10}H_{194}N_2Ni$: C 74.83, H 10.99, N 1.59, Ni 3.33. Found C 74.32, H 11.08, N 1.54, Ni 3.10.

General Procedure for 7a, n = 14. To 0.20 g (0.1 mmol) of **16** in 4 mL of THF was slowly added a hot 42 mg (0.1 mmol) of cupric perchlorate hexahydrate in 16 mL methanol. The resulting solution was refluxed for 3 h and cooled, and excess methanol was added to precipitate the product which was filtered, washed with methanol, and recrystallized from THF/acetone to give a brown powder, 0.13 g (67% yield). IR (thin film) 2917, 1575, 1533, 1516, 1490, 1472, 1435, 1388, 1332, 1261, 1224, 1179, 1117, 1038, 918, 862, 802, 719 cm^{-1}. MS 1823 (M^+). Anal. Calcd for $C_{110}O_{10}H_{192}N_2CuNi$: C 72.37, H 10.61, N 1.54, Cu 3.48, Ni 3.22. Found C 71.95, H 10.43, Cu 3.46, Ni 3.13.

7b, n = 14. This bimetallic complex was prepared using the same procedure as in the preparation of **7a** (n = 14) except that palladium acetate was used to give an orange/brown powder in 65% yield. IR (thin film) 2912, 1570, 1525, 1502, 1471, 1436, 1377, 1331, 1244, 1223, 1175, 1113, 1038, 989, 854, 783, 719 cm^{-1}. MS 1869 (M^+). Anal. Calcd for $C_{110}O_{10}H_{192}N_2NiPd$: C 70.62, H 10.35, N 1.50, Cu 3.40, Pd 5.69. Found C 70.56, H 10.14, N 1.37, Cu 3.23, Pd 5.53.

7c·MeOH. This bimetallic complex was prepared using the same procedure as in the preparation of **7a** (n = 14) except that nickel acetate tetrahydrate was used to give a brown powder in 44% yield. IR (thin film) 3347, 2943, 1576, 1490, 1470, 1456, 1446, 1430, 1379, 1333, 1220, 1173, 1117, 1042, 1015, 992, 890, 850, 761, 722 cm^{-1}. MS 1818 (M^+). Anal. Calcd for $C_{110}O_{10}H_{192}N_2Ni_2$·MeOH: C 72.00, H 10.68, N 1.51, Ni 6.27. Found C 72.43, H 10.41, N 1.35, Ni 6.21.

7d·MeOH. This bimetallic complex was prepared using the same procedure as in the preparation of **7a** (n = 14) except that manganese perchlorate hexahydrate was used to give a brown powder in 67% yield. IR (thin film) 3390, 2917, 1575, 1494, 1466, 1429, 1378, 1333, 1229, 1173, 1117, 1038, 1013, 992, 848, 762, 722 cm^{-1}. MS 1815 (M^+). Anal. Calcd for $C_{110}O_{10}H_{192}N_2NiMn$·MeOH: C 72.12, H 10.70, N 1.52, Ni 3.14, Mn, 2.98. Found C 70.56, H 10.14, N 1.37, Ni 3.17, Mn 2.85.

7e·MeOH. This bimetallic complex was prepared using the same procedure as in the preparation of **7a** (n = 14) except that cobalt acetate tetrahydrate was used to give a brown powder in 56% yield. IR (thin film) 3411, 2918, 1574, 1496, 1465, 1436, 1379, 1333, 1229, 1222, 1174, 1117, 1038, 862, 783, 723 cm^{-1}. MS 1819 (M^+). Anal. Calcd for $C_{110}O_{10}H_{192}N_2NiCo$·MeOH: C 71.96, H 10.67, N 1.51, Ni 3.13, Co 3.19. Found C 70.56, H 10.14, N 1.37, Ni 3.02, Co 2.93.

Acknowledgment. We are grateful for financial support provided by the National Science Foundation (DMR-9258298 and DMR-9119045) and the Office of Naval Research. We are also thankful for funds provided by the Office of Naval Research, the University of Pennsylvania, and the Laboratory for Research on the Structure of Matter (DMR-9120668) for funds used to create a variable-temperature XRD facility. A.G.S. is a Ford Foundation Predoctoral Fellow and is appreciative of a Gloria Twine Chisum Fellowship.

Supplementary Material Available: Tables of crystal coordinates, additional ORTEP views, thermal parameters, bond distances, F_{obs} and F_{cal}, and bond angles of **IIIb** (n = 6) (22 pages); list of F_{obs} and F_{cal} (58 pages). Ordering information given on any current masthead page.